

OPEN ACCESS

EDITED BY

Antonios Kanellopoulos, University of Hertfordshire, United Kingdom

DEVIEWED BY

Mahmoud Ebrahimi, University of Maragheh, Iran Jun-Jie Zeng, Guangdong University of Technology, China

*CORRESPONDENCE

Libin Jiao,

iaolibin@petrochina.com.cn

 iaolibin@petrochina.com.cn

RECEIVED 12 July 2025 ACCEPTED 02 September 2025 PUBLISHED 30 September 2025

CITATION

Luo Z and Jiao L (2025) Experimental, computational, and simulation methods for investigating the pore connectivity of cement-based materials: a review.

Front. Mater. 12:1664496.
doi: 10.3389/fmats.2025.1664496

COPYRIGHT

© 2025 Luo and Jiao. This is an open-access article distributed under the terms of the Creative Commons Attribution License (CC BY). The use, distribution or reproduction in other forums is permitted, provided the original author(s) and the copyright owner(s) are credited and that the original publication in this journal is cited, in accordance with accepted academic practice. No use, distribution or reproduction is permitted which does not comply with these terms.

Experimental, computational, and simulation methods for investigating the pore connectivity of cement-based materials: a review

Zhiyuan Luo¹ and Libin Jiao²*

¹School of National Defense and Nuclear Science and Technology, Mianyang, China, ²Engineering Technology Research Institute, PetroChina Southwest Oil & Gas Field Company, Chengdu, China

Pore connectivity (β) is a key parameter for investigating the hydration mechanism, transport performance, corrosion mechanism, and durability of cement-based materials. This article reviews the general experimental and computational, and numerical simulation methods used to study the β of cement-based materials. The principles, characteristics, and application of traditional and advanced experimental methods used to study the β of cement-based materials are compared and analysed. The principles and research progress of computational models, including random walker algorithm, Archie's law, and multi-phase phenomenological model, are summarised. The characteristics of numerical simulation methods, such as hydrationmorphology-structure, CEMHYD3D, and HydratiCA, are described. Additionally, the research progress, challenges, and directions with respect to the β of cement-based materials are comprehensively discussed. This review aims to provide some foundation for understanding the pore structure, hydration and corrosion mechanism and for developing a durability prediction model of cement-based materials in the future.

KEYWORDS

pore connectivity, cement-based materials, durability, evaluation method, hydration mechanism

1 Introduction

Cement-based materials are the most widely used artificial materials, and their total annual production is over 20 billion tons; however, the CO₂ emission during the production of the materials accounts for 5%–10% of the world's total CO₂ emission (Abdolhosseini Qomi et al., 2014; Zhang W. et al., 2020; Jiang et al., 2025; Sun et al., 2025). Thus, to reduce the impact of the production of cement-based materials on the environment, improving the corrosion resistance and durability of the materials is an effective measure. However, there are a large number of complex pore structures in cement-based materials, which seriously affect the durability of the materials (Wang W. et al., 2019; MacLeod et al., 2020; Upshaw and Cai, 2020; Zhang W. et al., 2020; Yu et al., 2024; Papp et al., 2025). Furthermore, the connected pores in the materials can provide a flow channel for the migration of water (Cao et al., 2019), Ca²⁺ ions (Gaitero et al., 2008), and corrosive medium (Zhang, 2017). Therefore, a generally acceptable view is that the pore structure, especially

pore connectivity (β), is a key parameter to investigate the durability of hardened cement-based materials (Zhang et al., 2018b; 2018c; Cao et al., 2019; Li et al., 2019). Meanwhile, researchers (Li Z. et al., 2016; Lyles, 2016) have proposed that understanding the pore structure and β of cement slurry during the hardening stage is very important to investigate the "natural gas migration" behavior in the cement slurry, and develop an anti-natural gas-migration technique for the cementing engineering of natural gas wells.

Based on the pore size, the pores in cement-based materials are divided as gel pores, capillary pores, and macropores (Liu et al., 2019b). The macropores contain hollow-shell pores (Bede et al., 2016; Tang et al., 2016) and air voids. Generally, the volume fraction of macropores in cement-based materials is low, and these pores have poor connectivity. Air voids are formed by air entrainment during the preparation of cement-based materials, which are entrapped and have a large diameter. Previous studies (Hadley et al., 2000; Aligizaki, 2006) have reported that the hollowshell pores are formed by hollow-shell hydration grains. The pores in the hydration products are named as gel pores, which have poor connectivity and their size is less than 10 nm. According to the microstructure of calcium silicate hydrates (C-S-H), Bede et al. (Bede et al., 2016) categorised gel pores into intra C-S-H gel pores (0.5-1.8 nm) and inter C-S-H pores (2-10 nm). Capillary pores are widely distributed in the hydration products, do not have a regular shape, and have size larger than 50 nm (Bede et al., 2016). Under natural conditions, the capillary pores are filled with pore solution and thus impact the durability of cement-based materials (Tang et al., 2016; Zhang et al., 2018b).

Recently, researchers have established several prediction models of capillary porosity (ϕ) and connectivity in cement-based materials using traditional methods such as mercury intrusion and gas adsorption (Salmas and Androutsopoulos, 2001; He et al., 2018). Furthermore, some advanced experimental methods, including highresolution computed tomography (CT) (Yue et al., 2025), nuclear magnetic resonance (NMR) (Yu et al., 2024; Song et al., 2025b), and electrical techniques, have been used for the in situ testing of the β in cement-based materials (Tang et al., 2016; 2017; Liu et al., 2019b). Moreover, with the development of mathematical theories and computing technologies, researchers have constructed some numerical simulation methods to predict the hydration process, microstructure, pore structure, and properties of these materials (Breugel, 1995; Bentz, 2005). Based on these research achievements, several reviews have been reported on the pore structure of cementbased materials. For example, Diamond (Diamond, 2000) reviewed the experimental processes and conditions of mercury intrusion to analyse the pore structures of cement-based materials. Tang et al. (Tang et al., 2016; Tang et al., 2017) reviewed the research processes used and the challenges encountered in the study of the pore structures of these materials using electrical methods such as electrical impedance and direct and alternative current methods. Zhang (Zhang and Zhang, 2014) reviewed the transport performance, ion diffusion, and gas permeability of unsaturated cement-based materials and reported the effects of chloride binding, supplementary cementitious materials, and water-to-cement ratio (W/C) on the transport performance of the materials. Patel et al. (Patel et al., 2016) evaluated the experimental and simulation methods used to investigate the effective diffusion coefficients (D(Δ)) in saturated cement-based materials. Garboczi et al. (Garboczi, 1990) reviewed the principles and applications of several computational theories, such as Archie's Law, Katz–Thompson theory, and Kozeny–Carman theory, and models for predicting the permeability of porous materials. Thomas et al. (2011) examined numerical simulation models, including single-particle, mathematical nucleation-growth, and vector and lattice-based models, used to predict the complex hydration reaction and microstructure of cement-based materials. Although β is a key parameter to investigate the corrosion behavior and predict the durability of cement-based materials, these reviews have paid little attention to the experimental, computational, and numerical methods used to test the β of cement-based materials and the research progress and challenges in the study of the β of these materials.

Therefore, the purpose of this review is to summarise the principles, characteristics, and applications of the experimental, computational, and simulation methods used to study the β in cement-based materials. Figure 1 presents the outline of this review. According to the underlying principles and sample preparation techniques, the experimental methods used to study β are divided into traditional and advanced experimental methods. Traditional methods include mercury intrusion, gas adsorption, and direct imaging methods, and advanced methods comprise high-resolution CT, NMR, and electrical methods. Herein, we have comparatively analysed the principles, characteristics and applications of these experimental methods, summarised the computational methods used to calculate the β in cement-based materials, and described the numerical simulation techniques applied to predict the microstructure and pore structure of these materials. Finally, the challenges and directions in the study of the β of these materials are evaluated.

2 Traditional experimental methods for testing the β

To study the β in hardened cement-based materials, researchers have established computational models based on the results of mercury intrusion and gas adsorption. Zeng et al. (Zeng et al., 2012; He et al., 2018) proposed that pore entrapment is the key parameter to determine the β in cement-based materials, and the volume fraction of the entrapped pores (α_{en}) can be expressed as Equation 1

$$\alpha_{en} = \frac{V_{en}}{V_{t}} \tag{1}$$

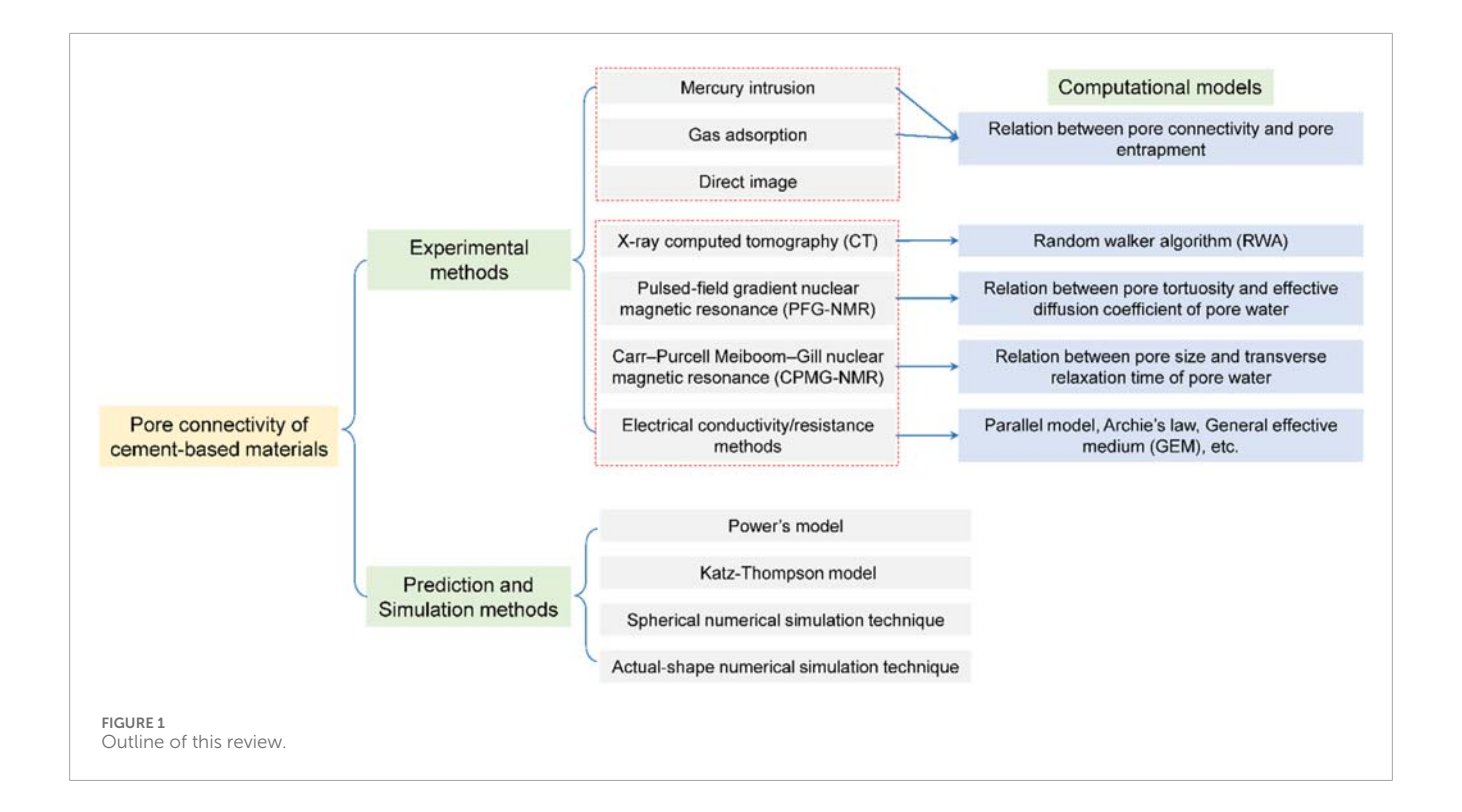
where V_{en} and V_{t} are the volumes of the entrapped pores and total volume of pores, respectively. Salmas et al. (Salmas and Androutsopoulos, 2001) formulated a relationship between α_{en} and pore tortuosity (τ), which can be expressed as Equation 2

$$\tau = 4.6242 \ln \left(\frac{4.996}{1 - \alpha_{en}} - 1 \right) - 5.8032 \tag{2}$$

According to the experimental results and multi-phase phenomenological model, He et al. (He et al., 2018) described a relationship between β and τ as follows Equation 3:

$$\beta = \frac{1}{\tau^{1.721}} \tag{3}$$

Based on the abovementioned computational models, α_{en} is an important parameter to calculate the β . Moreover, mercury intrusion and gas adsorption are effective methods to investigate the α_{en} of cement-based materials.



2.1 Mercury intrusion

Mercury intrusion is used to determine the pore structure (φ , pore size distribution, and pore surface area) of a material by recording the mercury injection volume under different pressures (Li et al., 2025b; Dai et al., 2024). The pore shape in cement-based materials is assumed to be cylindrical. According to the surface tension of mercury ($\chi_m = 0.485 \text{N/m}$) and contact angle between mercury and cement-based materials ($\theta = 130^\circ$), the relationship between the mercury injection pressure (P_i) and pore diameter (D_m) can be expressed as Equation 4 (Zhou et al., 2017) Equation 4.

$$D_{\rm m} = -\frac{4\chi_{\rm m}\cos\theta}{P_{\rm i}} \tag{4}$$

He et al. (He et al., 2018) determined the α_{en} by calculating the difference between the volumes of the intruded and extruded mercury (Figure 2). Additionally, to accurately analyse the pore structure of cement-based materials by mercury intrusion, the sample need be dried to remove the pore water (Galle, 2001). According to Equation 4, mercury intrusion investigates the pore structure under high pressures. However, the drying and high pressure may change the skeleton in the sample.

2.2 Gas adsorption

Gas adsorption is employed to measure the pore size using capillary condensation and volume equivalence principles. In this method, the volume of the gas filled in the pores is considered equivalent to the pores volume. The gas can be nitrogen, steam, or carbon dioxide. During gas adsorption, the pore size determined by capillary condensation is different under different relative pressures

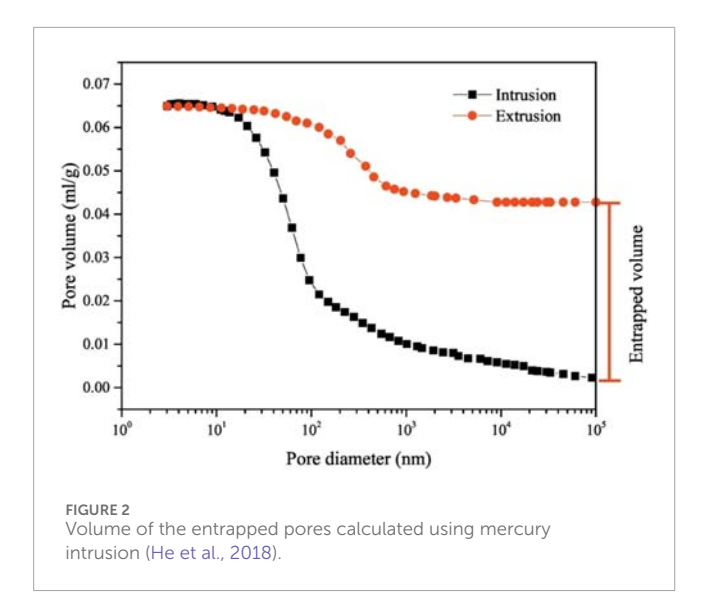
 (P/P_0) , and it reduces with an increase in the P/P_0 . Therefore, Brunauer, Emmett, and Teller used classical statistical theory to deduce a multilayer adsorption equation (Brunauer et al., 1938) and determined the relationship between the P/P_0 and specific surface area of pores by a method named as Brunauer–Emmett–Teller method. Barrett, Joyner, and Halenda proposed a relationship between the P/P_0 and critical pore radius, as shown in Equation 5, using a method called Barrett–Joyner–Halenda (BJH) method (Zhou et al., 2017).

$$r_{c} = \frac{2\chi V}{RT \ln \left(P/P_{0} \right)} \tag{5}$$

where r_c , χ , R, T, V, and P/P_0 are the critical pore radius, surface tension of gas, gas constant, absolute temperature, molar volume of gas, and relative pressure, respectively. Salmas et al. (Salmas and Androutsopoulos, 2001) determined the α_{en} by analysing the adsorption and desorption results.

2.3 Direct imaging method

Backscatter scanning electron microscopy (BSEM) and scanning electron microscopy (SEM) are used to directly observe the pore structure of cement-based materials (Scrivener, 1988; Wong et al., 2006; Attari et al., 2016; Lyles, 2016; Liu et al., 2019a; Xu et al., 2021; Dong et al., 2024; Song et al., 2025a). The main experimental procedure includes: 1) the sample is dried to remove the pore water; 2) a resin or low-melting-point metal is injected into the pores under high pressure or vacuum conditions (Chen et al., 2017); 3) when the resin or the metal is hardened, the sample with the resin or the metal is polished to obtain a flat surface; and 4) BSEM is used to obtain the corresponding images. Subsequently, the BESM images



are treated as binary images, and the grey threshold value between the pores and solid phase is calculated using the entropy determined by the grey-level histogram (PUN, 1980), indicator kriging (Oh and Brent Lindquist, 1999), global threshold (Ranefall and Wählby, 2016), inflection point (Wong et al., 2006; Liu et al., 2019a), and ISODATA threshold (Ridler and Calvard, 1978; Chen et al., 2017) methods. According to the grey threshold value, the areas of the pores and solid phase can be evaluated to obtain the ϕ and pore size (Figure 3). Furthermore, the SEM images of the sample can be used to analyse the pore structures using the grey threshold value method (Attari et al., 2016; Liu et al., 2019a; 2020c; Zhang X. et al., 2020) (Figure 4). The methods via which the pore structures of a sample can be directly determined by the BESM or SEM images are named as direct imaging methods. Moreover, using the direct imaging methods, the β can be directly obtained in two-dimensions. Additionally, to investigate the three-dimensional (3D) β of cementbased materials, some researchers have used stereological methods to create a 3D microstructure of these materials using the BESM or SEM images (Mrzygłód et al., 2013; Li T. et al., 2016).

However, according to the abovementioned analysis, sample preparation in traditional experimental methods involves drying of the sample. Researchers (Galle, 2001; Zhang and Scherer, 2011; Zhang et al., 2019) have investigated the effects of drying methods (including 65 °C vacuum drying for 24 h (65VD), 105°C oven drying for 24 h (105D), ethanol solvent-exchange for 3 days +50°C oven drying for 24 h (A50D), and freeze-drying with liquid nitrogen (FD)) on the pore structures in cement-based materials using nitrogen adsorption and BJH methods; the experimental results show that the pore size and ϕ of the dried sample significantly increased when compared with those of the non-dried sample. Additionally, the pore structures of the cement-based materials dried by different methods have clear differences, and after 105D, the content of the macropores in these materials obviously increased (Figure 5). Fourmentin et al. (Fourmentin et al., 2017) proposed that the removal of pore water from these materials changes the C-S-H microstructure, and the pore size of the sample is increased (Figure 6).

3 Advanced experimental methods for testing the β

To avoid damaging the pore structure in cement-based materials during drying, some *in situ* nondestructive methods, such as high-resolution CT, NMR, and electrical methods, have been applied to test the pore structures and β of the materials (Wang X. et al., 2019).

3.1 X-ray CT

3.1.1 CT principle

According to Beer's law (Sukop et al., 2008; Moreno-Atanasio et al., 2010), the absorptivity of a sample to monochromatic X-rays depends on the density of the sample (ξ), atomic number (N), and electron beam energy (E). Therefore, when a monochromatic X-ray passes through a heterogeneous sample with i components, the intensity of the X-ray can be expressed as Equation 6:

$$I = I_0 \cdot \exp\left[\sum_i -\mu_i x_i\right] \tag{6}$$

where I_0 , I, μ_i , and x_i are the initial intensity of the monochromatic X-ray, intensity of the X-ray after it passes through the sample, absorption coefficient of the ith component, and length of the sample, respectively. Moreover, the μ_i is determined by ξ , N, and E, and their relationship can be expressed as Equation 7

$$\mu_{\rm i} = \xi \left(a + \frac{bN^{3.8}}{E^{3.2}} \right) \tag{7}$$

where a is a low-energy-dependence parameter and b and E are constants. According to the abovementioned principles, when monochromatic X-rays pass through a material with high density, the material will absorb more X-rays. The X-ray intensity signal obtained by a CCD detector will be weakened (Sukop et al., 2008; Fusseis et al., 2014). Then, the X-ray intensity signal acquired by the CCD detector will be treated and saved as a data matrix. Using this data matrix and image reconstruction technology, the microstructure of the sample can be obtained (Zhang et al., 2012; Wildenschild and Sheppard, 2013).

To date, high-resolution CT is widely used to investigate the microstructure, pore structure, and β of cement-based materials (Sugiyama et al., 2016). For example, Hong et al. (Hong et al., 2019) used micro-CT to directly observe the 3D crack microstructure in cement mortar and found that the fracturing process of the mortar includes compression, expansion, and cracking stages; this observation is consistent with the compression failure process fracture theory. Suleiman et al. (Suleiman et al., 2019) examined the 3D microstructure and cracks volume in self-healing cementbased materials during the self-healing process using micro-CT. They studied the effects of mineral addition on the healing efficiency of these materials and found that the cement-based materials containing limestone microfiller have higher healing efficiency than those of the materials with other minerals. Additionally, a combination of micro-CT and random walker algorithm (RWA) has been used to analyse the 3D microstructure and pore network characteristics of alkali-activated binders, and researchers have found that the diffusion tortuosity of the binders is related to their φ (Provis et al., 2012).

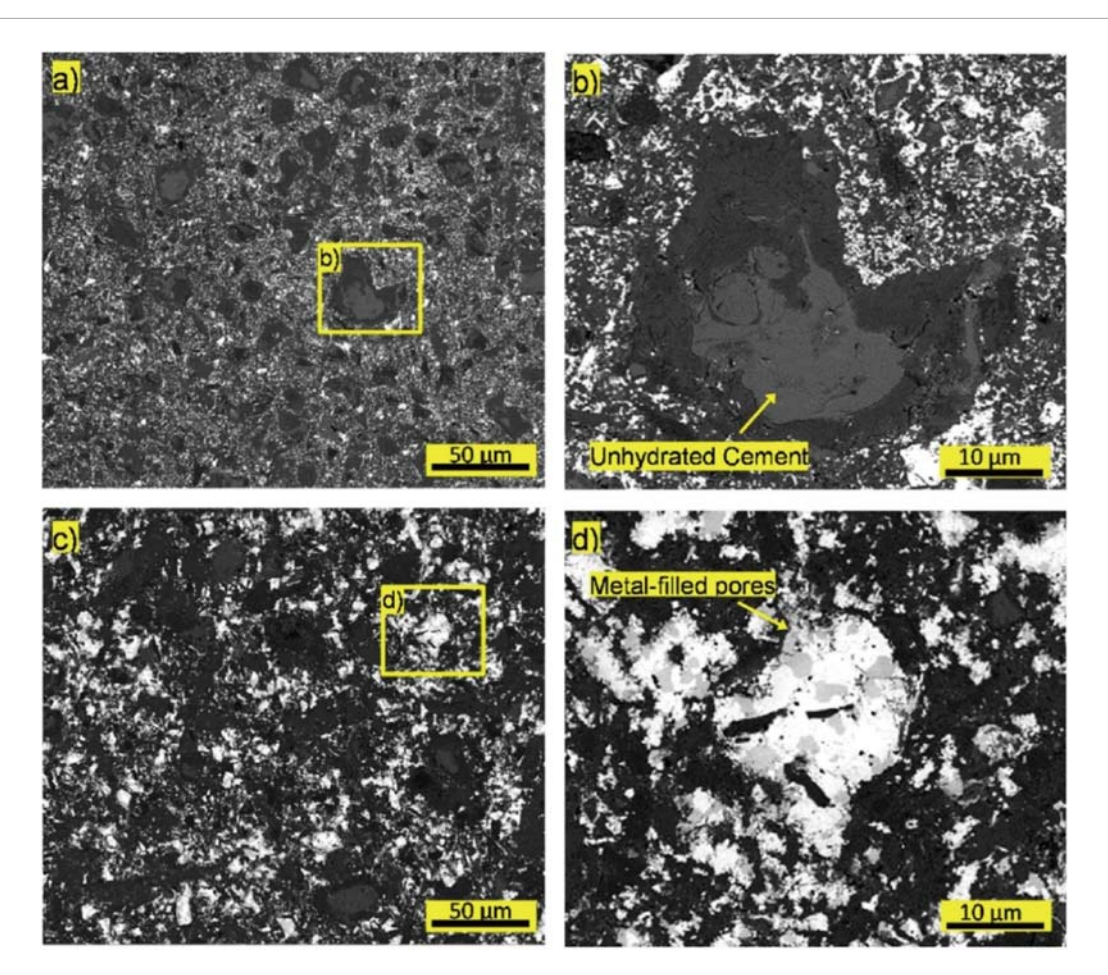


FIGURE 3
BSEM images of cement-based materials (The white area is pores. The black and grey areas are solid phases) (Chen et al., 2017). (a) sample C1, w/c = 0.4, 10 cycles,15.2 MPa; (b) magnified BSE image for pores near an unhydrated cement grain; (c) sample C2, w/c = 0.8, 4 cycles, 15.2 MPa; (d) magnified BSE image of large metal-filled pores.

3.1.2 τ analysis

According to Equation 3, the τ of cement-based materials is related to their β . Therefore, to study the τ of cement-based materials, Nakashima et al. (Nakashima and Watanabe, 2002; Nakashima and Kamiya, 2007) reported the principle of RWA to calculate the τ . From the entire CT data, the RWA randomly selects a pore voxel as a walker, and the walker is used as a starting point of the lattice walk trial at t=0. Then, the walker randomly jumps to the nearest other pore voxels. After the walker jumps, t increases to t+1. If the randomly selected voxel is solid, no jumping is performed; however, the t still increases to t+1. Therefore, the mean-square displacement ($\langle \tau^2 \rangle$) of the walker can be expressed as Equation 8

$$\left\langle r(t)^{2}\right\rangle =\frac{1}{n}\sum_{i=1}^{n}\left[\left(x_{i}(t)-x_{i}(0)\right)^{2}+\left(y_{i}(t)-y_{i}(0)\right)^{2}+\left(z_{i}(t)-z_{i}(0)\right)^{2}\right] \tag{8}$$

where n, t, and $x_i(t)$, $y_i(t)$, and $z_i(t)$ are the number of random walkers, dimensional integer time, and positions of the *i*th walker in the x, y, and z directions, respectively, at t. If the walker is in a space without solid (i.e., ϕ is 100%), the $\langle r^2 \rangle$ of the walker is Equation 9

$$\langle r^2 \rangle_{\text{free}} = 6D(0)t = \alpha^2 t$$
 (9)

where D(0) is the diffusion coefficient of the walker in free space and α is the lattice constant of the cube voxel. Furthermore, in isotropic homogeneous porous materials, the diffusion coefficient (D(t)) (scalar) is related to the time-derivative of its $\langle r^2 \rangle$ as Equation 10:

$$D(t) = \frac{1}{6} \frac{d\langle r^2 \rangle}{dt}$$
 (10)

Therefore, the τ of porous materials can be determined by calculating the ratio of D(0) to D(t) (Nakashima and Kamiya, 2007) Equation 11:

$$\tau = \frac{D(0)}{D(t)} = \frac{\alpha^2}{\frac{\underline{d}\langle r(t)^2 \rangle}{dt}}, \text{as } t \to \infty$$
 (11)

If the pores in porous materials are anisotropic, their D(t) is a tensor (not a scalar) variable. The $\langle r^2 \rangle$ of the walker in the x, y, and z directions can be expressed as Equation 12. Additionally, in free space, the $\langle r^2 \rangle$ of the walker can be calculated by Equation 13. By combining Equation 12 and Equation 13, the τ of anisotropic porous materials can be determined.

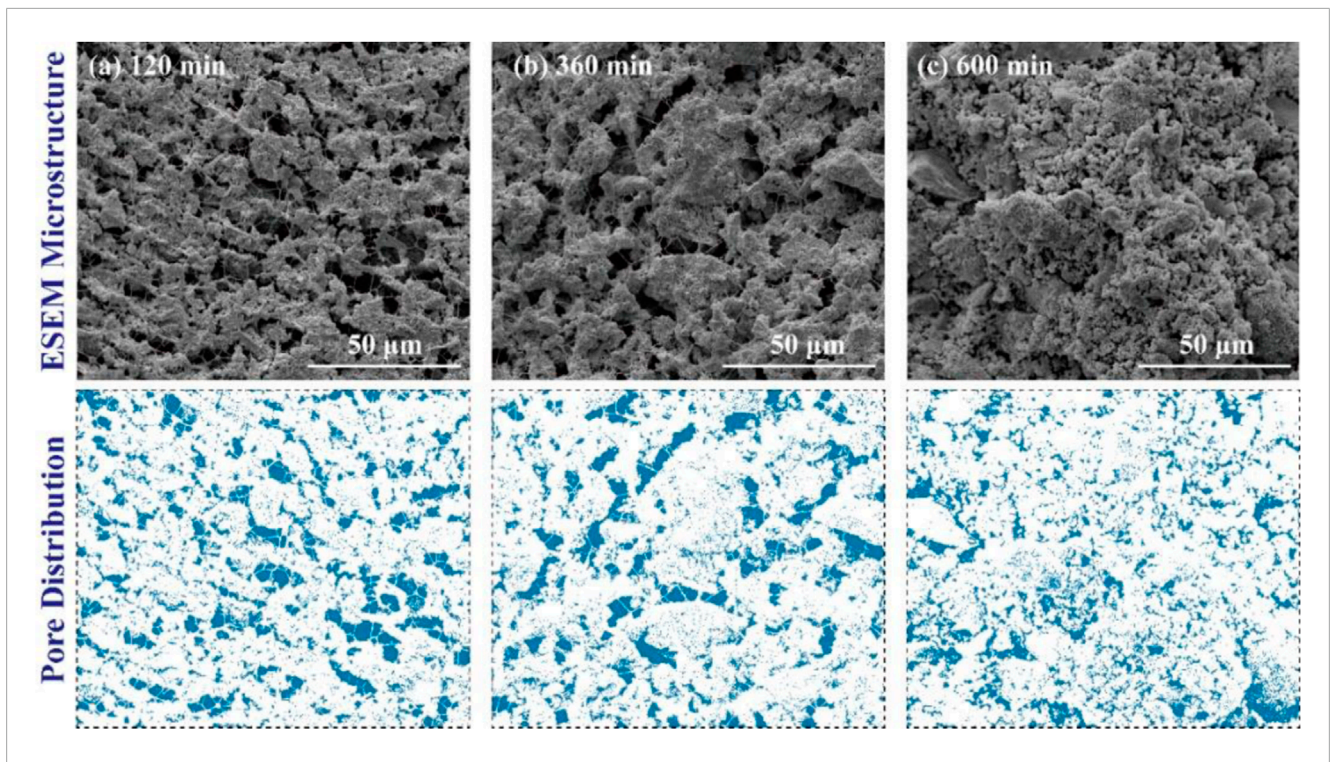
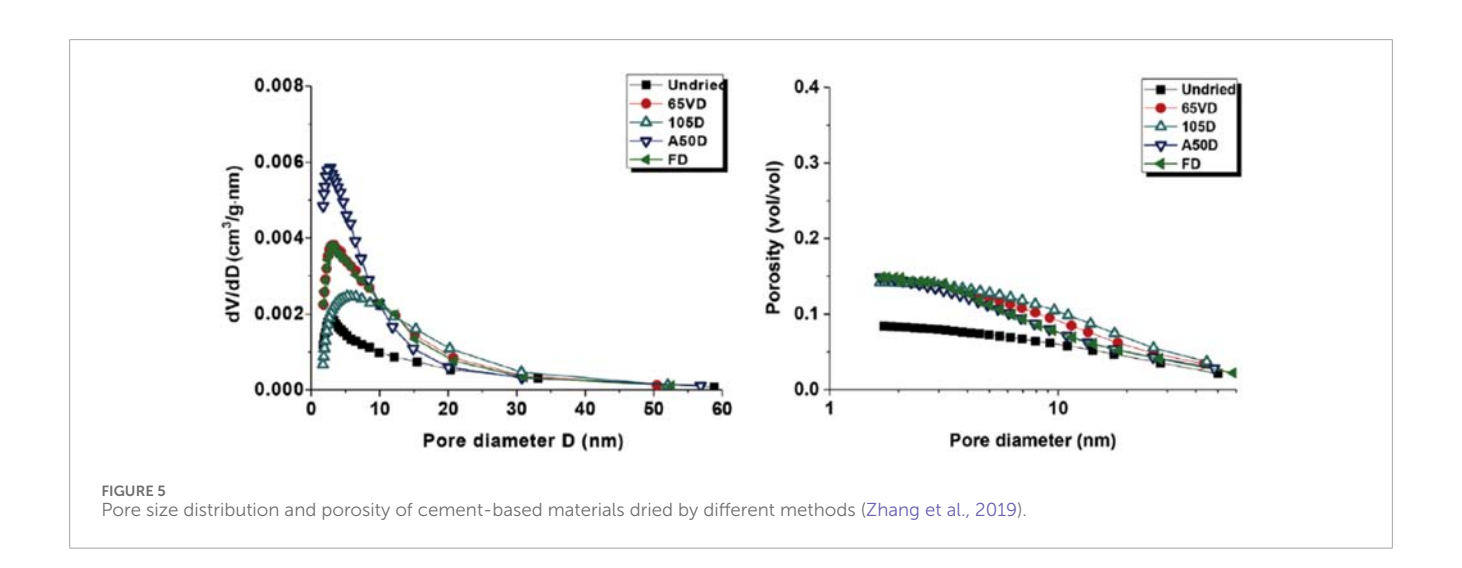


FIGURE 4
Pore structures of cement slurry in the early hydration stage (The blue area is pores) (Liu et al., 2019a). (a) 120 min. (b) 360 min. (c) 600 min.

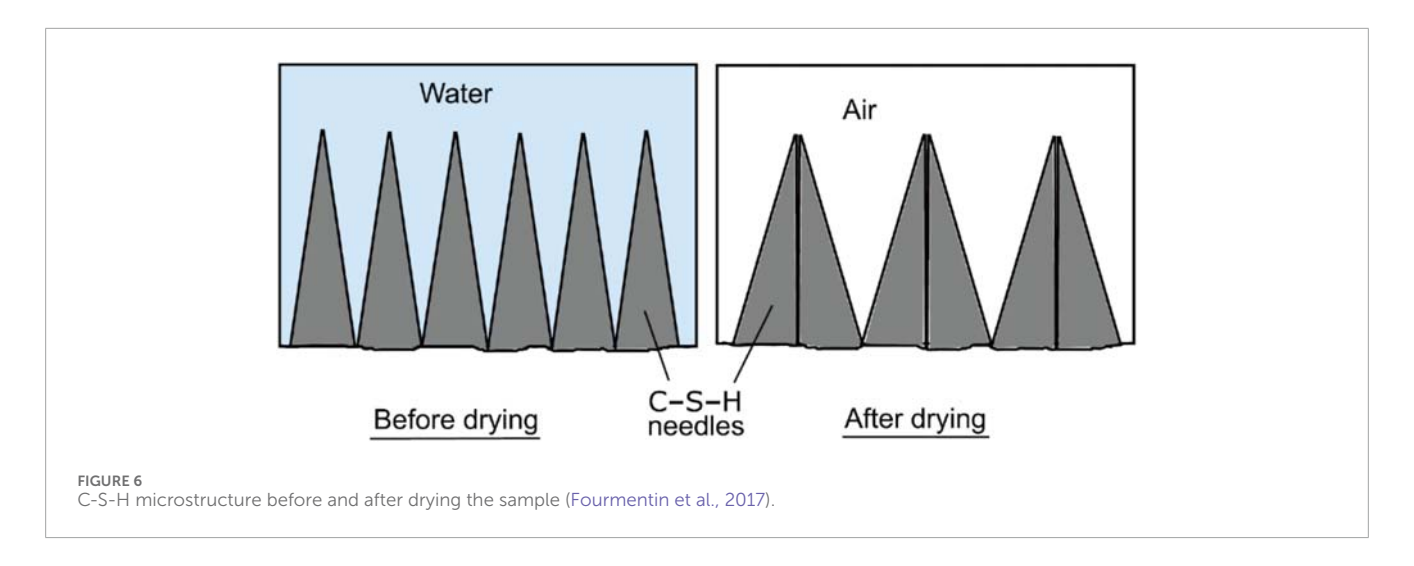


$$\begin{cases} \langle x(t)^2 \rangle = \frac{1}{n} \sum_{i=1}^{n} (x_i(t) - x_i(0))^2 \\ \langle y(t)^2 \rangle = \frac{1}{n} \sum_{i=1}^{n} (y_i(t) - y_i(0))^2 \\ \langle z(t)^2 \rangle = \frac{1}{n} \sum_{i=1}^{n} (z_i(t) - z_i(0))^2 \end{cases}$$
(12)

$$\langle x^2 \rangle_{\text{free}} = \langle y^2 \rangle_{\text{free}} = \langle z^2 \rangle_{\text{free}} = \frac{1}{3} \langle r^2 \rangle_{\text{free}} = \frac{1}{3} \alpha^2 t$$
 (13)

Using high-resolution CT, not only the 3D pore structures in cement-based materials can be directly observed, but also computational fluid dynamics (CFD) and lattice Boltzmann method

(LBM) can be applied to calculate the transport performance of water and ions and analyse the permeability and diffusion process of cement-based materials (Koivu et al., 2009; Oesch et al., 2018; Yang X. et al., 2019; Liu et al., 2020b; Li et al., 2025a; Pan and Gencturk, 2025). For example, based on the 3D microstructure investigated by high-resolution CT, Koivu et al. (Koivu et al., 2009) built an effective approach to calculate the diffusion, heat conduction, and permeability of cement-based materials using LBM and finite difference methods. Yang et al. (Yang X. et al., 2019) used micro-CT to examine the microstructure of G-class oil-well cement paste cured at 50°C under 10 MPa, and by combining



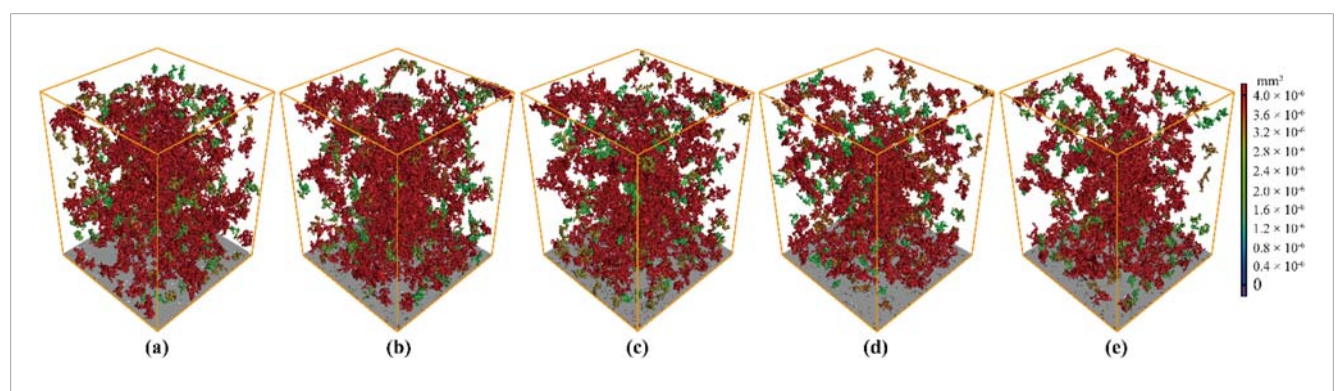


FIGURE 7
3D macroporous structure and spatial distribution of cement slurry in the early hydration stage (Liu et al., 2019b). (a) Hydration 4 h. (b) Hydration 6 h. (c) Hydration 8 h. (d) Hydration 10 h. (e) Hydration 12 h.

micro-CT with the CFD, they found that the permeability of the cement was 9.771 × 10-17 m2. Moreover, according to the 3D capillary pores of cement-based materials studied by micro-CT, researchers (Zhang et al., 2012; Zhang and Jivkov, 2016; Zhang, 2017) have comparatively calculated the water permeability and gas permeability of these materials and found that in these materials, the water permeability reduces and gas permeability increases with a decrease in saturation. Additionally, micro-CT has been utilized to investigate the hydration mechanism of Portland cement. Some researchers used micro-CT to in situ test the microstructure of the hydration products and the pore structure of cement slurry during hydration induction and acceleration periods (Figure 7) (Liu et al., 2019b). Hu et al. (Hu et al., 2016) and Bullard et al. (Bullard et al., 2018) studied the hydration of tricalcium silicate. They used highresolution CT to in situ measure the volume and microstructure of unhydrated tricalcium silicate and hydration products in a 15 mmol/L Ca(OH)2 solution and found that in the hydration acceleration period, the volume of the hydration products is four times the initial sample volume.

However, due to the resolution limitation of the CT CCD detector, it is difficult to measure nanoscale and submicron structures using the existing CT technology. There are many nanoscale and submicron pores in cement-based materials

(Ye et al., 2002; Lyles, 2016; Liu et al., 2019b). Therefore, to fully understand the β of cement-based materials, many techniques may be needed.

3.2 NMR

NMR has been widely used to study the pore structures of porous materials (including rocks and cement-based materials) (Webber et al., 2013; Dalas et al., 2014; Karakosta et al., 2015; Zhou et al., 2016; 2017; Fourmentin et al., 2017; Zhang et al., 2018a; Papp et al., 2025). Because the relaxation time of chemically bonded water in hydration products is approximately 20 µs, which is far lower than that of ¹H in pore water (Hansen, 1986; Valckenborg et al., 2001), NMR analyses the pore structures of cement-based materials by testing the relaxation signal of ¹H in pore water. The NMR experiment does not need a dry sample; however, the sample has to be treated by vacuum saturation of water (W.P.Halperin et al., 1994; Barberon et al., 2003; Zhou et al., 2017), which is beneficial for investigating the pore structures of cement-based materials. Pulsed-field gradient nuclear magnetic resonance (PFG-NMR) focuses on the τ and connectivity of porous materials, and Carr-Purcell-Meiboom-Gill

nuclear magnetic resonance (CPMG-NMR) focuses on the pore size distribution (Latour et al., 1995).

3.2.1 PFG NMR

The diffusion of molecules with a nuclear magnetic signal (M) between pulsed magnetic-field gradients will decline the M. The M/M_0 index can be expressed as (Zecca et al., 2018; Yang K. et al., 2019) Equation 14

$$\frac{M}{M_0} = \exp\left[-D_0(\gamma g \psi)^2 \left(\Delta - \frac{\psi}{3}\right)\right] \tag{14}$$

where D_0 , M_0 , γ , g, Δ , and ψ are the self-diffusion coefficient of the molecules, NMR signal without an applied magnetic-field gradient, spin magnetic ratio of nucleus, amplitude of the magnetic-field gradient, time interval, and duration of a single magnetic-field gradient, respectively.

In porous materials, the flow of molecules is limited by solid phases. Previous studies (Zecca et al., 2018; Yang K. et al., 2019) have reported that the $D(\Delta)$ of molecules is related to the NMR decay signal as Equation 15

$$\frac{M}{M_0} = exp \left\{ -D(\Delta) \gamma^2 \left[\psi^2 \left(4t + 6\lambda - \frac{2\psi}{3} \right) g_a^{\ 2} + 2\lambda \psi (\psi_1 - \psi_2) g_a g_0 + \frac{4}{3} \lambda^3 g_0^{\ 2} \right] \right\} \tag{15}$$

where λ , g_a , g_0 , and ψ_1 , and ψ_2 are the time between the first two RF pulses, applied magnetic-field gradient, internal magnetic-field gradient, and the pre-pulse and post-pulse time, respectively (Zecca et al., 2018). Mitra et al. (Mitra et al., 1992) have proposed that the relationship between the $D(\Delta)$ of molecules, D_0 , pore surface (S), and pore volume (V) is (Latour et al., 1993; 1995) Equation 16

$$\frac{D(\Delta)}{D_0} = 1 - \frac{4}{9\sqrt{\pi}} \frac{S}{V} \sqrt{D_0 \Delta} - \mathcal{O}(D_0 \Delta)$$
 (16)

When Δ is small, the function $\mathcal{O}(D_0t)$ is almost zero. Therefore, Equation 16 can be expressed as (Zecca et al., 2018; Yang K. et al., 2019) Equation 17

$$\frac{D(\Delta)}{D_0} \approx 1 - \frac{4}{9\sqrt{\pi}} \frac{S}{V} \sqrt{D_0 \Delta}$$
 (17)

Using the two-point Pade' approximation, $D(\Delta)/D_0$ can be expressed as Equation 18

$$\frac{D(\Delta)}{D_0} = 1 - \left(1 - \frac{1}{\tau}\right) \times \frac{c\sqrt{\Delta} + (1 - 1/\tau)\Delta/\varpi}{(1 - 1/\tau) + c\sqrt{\Delta} + (1 - 1/\tau)\Delta/\varpi}$$
(18)

where ϖ is the dimension of time and c is equal to $\frac{4}{9\sqrt{\pi}}\frac{S}{V}\sqrt{D_0}$.

At present, PFG-NMR is used to measure the τ of cement-based materials. For example, using isotope exchange experiments and PFG-NMR, Hansen et al. (Hansen et al., 2005) found that the long-range diffusivity of pore water in hardened cement paste with a W/C of 1.0 is approximately $(1.1\pm0.3)\times10^{-10}\,\mathrm{m}^2/\mathrm{s}$. Nybo et al. (Nybo et al., 2019) applied PFG-NMR to investigate the diffusion coefficient of hydrogen ions in the pores of cement paste under an electric field, and they found that the diffusion coefficient of the hydrogen ions reduces with an increase in the hydration time. Meanwhile, Patural et al. (Patural et al., 2010) reported that a small amount of cellulose ether reduced the water mobility of cement mortar. Nevertheless, the PFG-NMR results showed that

the diffusion coefficient of water molecules in the cement paste with cellulose ether at an actual application concentration was not changed. Therefore, the reason for the reduction of water mobility may be that cellulose ether increased the viscosity of pore water, which increased the capillary suction of pore water and reduced the mobility.

3.2.2 CPMG-NMR

CPMG-NMR mainly focuses on the transverse relaxation time (T_2) of samples. According to the previously reported results (Bhattacharja et al., 1993; Mcdonald et al., 2005; Zhou et al., 2018), there is a multiple index relationship between total magnetization intensity and T_2 of cement-based materials, as shown in Equation 19.

$$M(t) = M_0 \sum_{i} f_i \exp\left(\frac{-t}{T_{2i}}\right), f_j = \frac{V_j}{V_t} \text{ and } \sum_{i} f_j = 1,$$
 (19)

where M(t), V_t , V_j , M_0 , and f_j are the total magnetization intensity, total volume of pore water in the sample, volume of j^{th} pore water, initial magnetization intensity, and volume fraction of the j^{th} pore water in the total pore water, respectively. In cement-based materials, the pore water can be divided as bulk water and surface water, and the T_2 can be expressed as Equation 20

$$\frac{1}{T_2} = \frac{v_s}{T_{2s}} + \frac{(1 - v_s)}{T_{2b}},\tag{20}$$

where T_{2b} , T_{2s} , and v_s are the transverse relaxation time of bulk water, transverse relaxation time of surface water, and volume fraction of surface water, respectively, and the volume fraction of bulk water is $(1-v_s)$. In a cement-based material, the volume of total pore water, the thickness of surface water, and the pore surface were hypothesized as v_w , δ , and S_c , respectively. Thus, $v_s = \delta \cdot S_c/v_w$. According to the literature results (Korb et al., 2007; Dalas et al., 2014), the T_{2b} is far larger than the T_{2s} ; therefore, Equation 20 can be approximated as Equation 21

$$\frac{1}{T_2} = \frac{\delta \cdot S_c}{T_{2s} \cdot v_w} + \frac{\left(1 - \delta \cdot S_c / v_w\right)}{T_{2b}} \approx \frac{\delta}{T_{2s}} \cdot \frac{S_c}{v_w},\tag{21}$$

Generally, the pore shape in cement-based materials is considered cylindrical; thus, Equation 22 can be obtained as

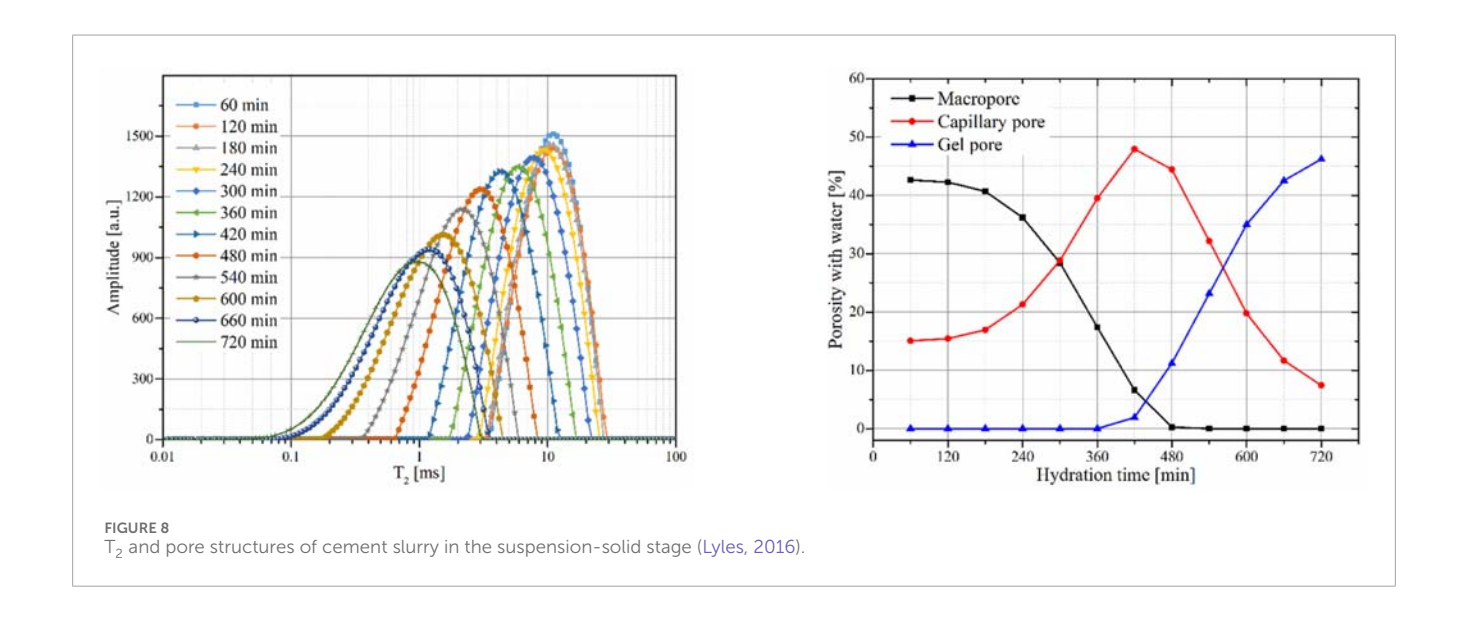
$$\frac{1}{T_2} = \epsilon \cdot \frac{2}{R},\tag{22}$$

where R is the pore radius and ϵ is the relaxivity of the hydration products in cement paste ($\epsilon = \delta/T_{2s}$). Dalas et al. (Dalas et al., 2014) measured the ϵ of each product in the cement paste using electron spin resonance, and the results are presented in Table 1. According to Equation 22, the T_2 is proportional to the R of cement-based materials.

CPMG-NMR has been widely used to investigate the pore structures of cement-based materials. For example, Bede et al. (Bede et al., 2016) classified the pores of cement-based materials into capillary, intra-C-S-H sheet, and inter-C-S-H gel pores. They comparatively studied the effects of different filling liquids (water, ethanol, and cyclohexane) on the pore structure analysis of cement-based materials and found that ethanol and cyclohexane could better distinguish the pore reservoirs of cement-based materials than

TABLE 1 Relaxivity and surface species density of each product in cement-based materials (Dalas et al., 2014).

Phase	Surface relaxivity (€)	Surface species density (ions/m²)	
C-S-H	5.51	19×10^{12}	
Ettringite	39.5	2.3×10^{14}	
Gypsum	6.2		
Crushed calcite	5.04	2.2×10^{17}	
Synthetic calcite	2.74	1.5×10^{15}	
Monocarboaluminate	1.65	7.4×10^{14}	



water. Liu et al. (Lyles, 2016) in situ measured the T_2 of cement slurry in a suspension-solid stage. According to the T_2 of cement slurry, they found that when the cement slurry was in the suspension-solid stage, the pore water changed into gel water and capillary water; this proved that during this stage, the macropores in the cement slurry change into gel and capillary pores (see Figure 8).

3.3 Electrical conductivity/resistance methods

Recently, some electrical conductivity/resistivity methods, including the direct current method (Tang et al., 2017; Long et al., 2019), alternating current method (Woo et al., 2005), alternating current impedance spectroscopy (McCarter et al., 2015; Kim et al., 2017), inductance conductivity (Liu et al., 2019b), non-contact resistivity measurement (Xiao and Li, 2008; He et al., 2018), and non-contact impedance measurement (Zhu et al., 2018), have been used to investigate the β of cement-based materials (Xiao and Li, 2008; Sanish et al., 2013; Ridha et al., 2014; Tang et al., 2016; Kim et al., 2017; Zhu et al., 2018). Tang et al. (Tang et al., 2017) reviewed the principles and procedures of these methods in detail.

In many previously reported studies, these methods have been used to explore the properties, microstructures, pore structures, and hydration degrees of cement-based materials (Christensen et al., 1994). For instance, Sanish et al. (Sanish et al., 2013) studied the setting process of cement paste with minerals and chemical admixtures and found that the electrical conductivity of the cement paste could predict the initial and final setting time of the cement paste; moreover, using a combination of Power's model (Bentz, 2006) and Archie's law (Roberts and Schwartz, 1985), the φ of the cement paste could be predicted. He et al. (He et al., 2018) replaced the pore water of the cement paste with a 3% NaCl solution and performed non-contact resistivity measurement to test the resistivity and formation factor (F) of the cement paste with different W/C. Then, a multi-phase phenomenological model, Archie's law, and GEM model were utilized to calculate the β of the cement paste. Their results showed that the β increased with an increase in the W/C. Zhu et al. (Zhu et al., 2018) used micro-CT and electrical conductivity methods to comparatively investigate the capillary φ of cement-based materials, and via the Archie's law, they found that at the same W/C, the τ of alkali-activated slag cement paste was lower than that of Portland cement paste. Moreover, the combination of micro-CT and electrical conductivity methods was used to analyse the relationship between the connected ϕ and β of

the cement slurry. The results indicated that the conductivity was proportional to the β of the cement slurry in the early hydration stage (Liu et al., 2019b). Additionally, the electrical methods were used to not only examine the pore structures and microstructures of cement-based materials, but also improve the conductivity of these materials. Cement-based materials with high conductivity can be applied as smart and multifunctional materials in practical engineering. Therefore, some high-conductivity materials, such as graphene (Wang D. et al., 2019), carbon nanofibers, and carbon nano-tubes (García-Macías et al., 2017; Kim et al., 2017; Sasmal et al., 2017), have been employed in these materials. Researchers have found that in cement-based materials, the dispersivity of the high-conductivity materials determines the conductivity.

3.3.1 Relationship between the F and capillary ϕ

Cement paste is a porous material, and the conductivity of its pore solution is significantly larger than that of solid hydration products. Some researchers have found that the conductivity of cement-based materials (σ) is determined by their β and pore solution (Liu et al., 2019b). The ratio of the resistivity of cement paste (ρ) and the resistivity of its pore solution (ρ_1) is called F (F = $\frac{\rho}{r}$). Many experimental results (Archie, 1941; Bernabé et al., 2011; He et al., 2018) have shown that F is a key parameter to describe the permeability and transport performance of cement-based materials. Moreover, based on different results, researchers have used the F of cement paste to establish several mathematical models for predicting capillary φ (Christensen et al., 1994; Zhang, 2008; He et al., 2018) (Table 2). Furthermore, based on experimental results, He et al. (He et al., 2018) analysed the match degree of these models (Table 2) and found that multi-phase phenomenological model, GEM, and Archie's model had better match with the experimental results than other models (Figure 9); this observation is consistent with the results reported in the literature (Oh and Jang, 2004; Nokken and Hooton, 2008; Zhang, 2008; Zhang and Li, 2009; Zhu et al., 2018).

3.3.2 Relation between ϕ , τ , and β

Christensen et al. (Christensen et al., 1994) hypothesized that only the pore solution of cement-based materials is conductive (i.e., the solid hydration products are insulators). The relationship between the σ , the conductivity of pore solution (σ_h) , and φ can be described as

$$\sigma = \sigma_{\rm b} \cdot \phi \cdot \beta \tag{23}$$

However, experiments have indicated that the solid hydration products are conductive. According to the experimental results, Shen and Chen (Shen and Chen, 2007) proposed a relationship between τ and F as Equation 24

$$\tau^2 = (F\phi)^n \tag{24}$$

where n is an empirical constant (n ranged from 0.91 to 1.20 (Shen and Chen, 2007; He et al., 2018)). According to the Archie's law, Equation 24 can be expressed as Equation 25

$$\tau^2 = \left(\mathbf{A} \cdot \mathbf{\phi}^{1-\mathbf{m}}\right)^{\mathbf{n}} \tag{25}$$

where A, m, and n are related to the properties of materials (A = n = 1 (van Brakel and Heertjes, 1974)).

Additionally, Iversen and Jorgensen (Iversen and Jørgensen, 1993) proposed that the ϕ was proportional to the square of τ (see Equation 26). Weissberg (Weissberg, 1963) described that the relationship between ϕ and τ is a logarithmic function (see Equation 27).

$$\tau^2 = \phi + B(1 - \phi) \tag{26}$$

$$\tau^2 = 1 - Y \ln \phi \tag{27}$$

where B and Y are empirical constants. Boundreau (Boudreau, 1996) determined that Y = 2, and Equation 27 can be expressed as Equation 28

$$\tau^2 = 1 + \ln \frac{1}{\phi^2}$$
 (28)

Moreover, based on the multi-phase phenomenological model (Archie, 1941), the relationship between ϕ and β can be determined, as shown in Equations 29, 30:

$$F = \frac{1}{\phi \cdot \beta} \tag{29}$$

$$\beta = \frac{1}{\tau^{2/n}} \tag{30}$$

4 Prediction models of β

4.1 Power's model

Researchers have realized that the density of hydration products is lower than that of unhydrated minerals, and the hydration products changes the pore structures and microstructure in cement-based materials. Therefore, the Power's model (Bentz, 2006) was established to describe the relationship between the pore solution fraction, the unhydrated cement fraction, and φ as follows Equations 31–33:

$$\phi_{w}(t) = \frac{\xi_{\text{cem}} \cdot (w/c) - \left(f_{\text{exp}} + \xi_{\text{cem}} \cdot \beta_{cs}\right) \cdot \alpha}{1 + \xi_{\text{cem}} \cdot (w/c)}$$
(31)

$$\phi(t) = \frac{\xi_{\text{cem}} \cdot (w/c) - f_{\text{exp}} \cdot \alpha}{1 + \xi_{\text{cem}} \cdot (w/c)}$$
(32)

$$\phi_{uh}(t) = \frac{1 - \alpha}{1 + \xi_{cem} \cdot (w/c)}$$
(33)

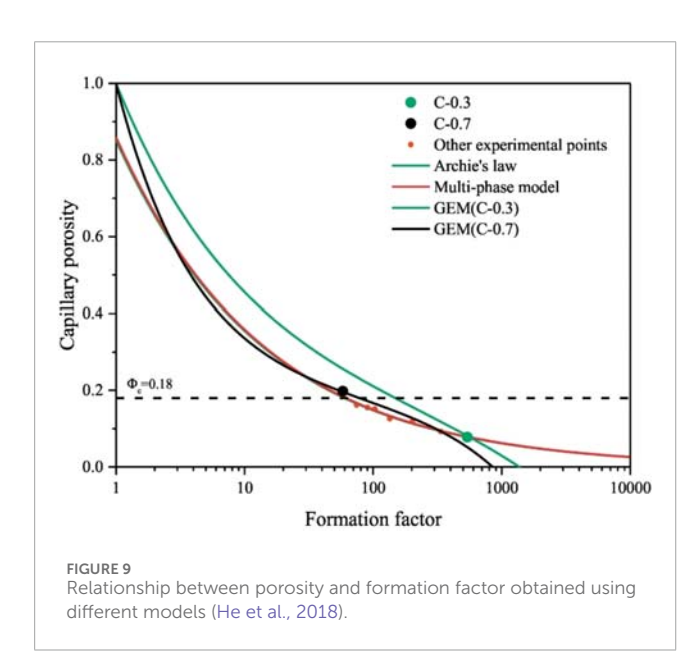
where $\phi_w(t)$, $\phi_{uh}(t)$, and $\phi(t)$ are the volume fraction of pore solution, volume fraction of unhydrated cement, and ϕ at time t, respectively; α , ξ_{cem} , f_{exp} , and β_{cs} are the hydration degree of the cement paste at time t, cement density, expansion coefficient of solid phases ($f_{exp} = 1.15$ (Sanish et al., 2013)), and chemical shrinkage parameter of cement paste ($\beta_{cs} = 0.07 \text{mL/g}$ (Bentz, 2006)), respectively.

4.2 Katz-Thompson model

Additionally, Katz and Thompson (Katz and Thompson, 1986) proposed a relationship between the permeability and conductivity

TABLE 2 Models used for describing the relationship between the conductivity, formation factor, and porosity of cement-based materials.

Models	Relationship between capillary porosity and resistivity	Formation factor (F)	Notes
Parallel model (Christensen et al., 1994)	$\frac{1}{\rho} = \frac{\varphi}{\rho_1} + \frac{1 - \varphi}{\rho_h}$	$F = \frac{\rho_h}{\rho_l(1\!-\!\varphi)\!+\!\rho_h}$	Ref. (Rajabipour and Weiss, 2007; Li et al., 2016a; He et al., 2018) also called multi-phase phenomenological model
Archie's law (Archie, 1941; Roberts and Schwartz, 1985; McLachlan et al., 1990; Christensen et al., 1994)	$\rho = \rho_l \cdot \varphi^{-m}$	$F = A \cdot \varphi^{-m}$	m is a tortuosity-related factor. $(1.3 \le m \le 4.0) \text{ (Bentz and Garboczi,} \\ 1992; \text{ He et al., 2018)}$
General effective medium (GEM) (McLachlan et al., 1990; Oh and Jang, 2004)	$\varphi = \frac{\left(\rho_h^{1/t} - \rho^{1/h}\right) \left[(1 - \varphi_c) \rho_1^{1/t} + \varphi_c \rho^{1/t} \right]}{\rho^{1/t} (\rho_h^{1/t} - \rho_1^{1/t})}$	$\begin{split} F = \left[m_{\varphi} + \sqrt{m_{\varphi}^2 + \frac{1 - \phi_c}{\phi_c} \left(\frac{\rho_h}{\rho_1} \right)^{1/t}} \right]^{-t} \\ (where m_{\varphi} = \\ \frac{1}{2} \left\{ \left(\frac{\rho_h}{\rho_1} \right)^{1/t} + \frac{\phi}{\phi_c} \left[1 - \left(\frac{\rho_h}{\rho_1} \right)^{1/t} \right] - \frac{1 - \phi_c}{\phi_c} \right\}) \end{split}$	$\varphi_c \approx 0.18$ (Zhang and Li, 2009)
NIST model (Bentz and Garboczi, 1992)	$\frac{\rho_{l}}{\rho} = 0.001 + 0.07 \varphi^{2} + H(\varphi - 0.18) \times \\ 0.18 \times (\varphi - 0.18)^{2}$	$F = \frac{1}{0.001 + 0.07 \varphi^2 + H(\varphi - 0.18) \times 0.18 \times (\varphi - 0.18)^2}$	H is a function H(x) = 1 for $x > 0$ and $H(x) = 0$ for $x \le 0$. (Garboczi and Bentz, 1998)
Percolation model (Keblinski and Cleri, 2004; Vertruyen et al., 2007)	$\rho = \rho_1 \cdot \left(1 - \frac{1 - \varphi}{1 - \varphi_c}\right)^{-m}$	$F = \left(1 - \frac{1 - \phi}{1 - \phi_c}\right)^{-m}$	m is a critical exponent
Series model (Zhang, 2008)	$\rho = \phi \rho_l + (1 - \phi) \rho_h$	$F = \varphi + \frac{\rho_h}{\rho_l} (1 - \varphi)$	
Effective medium model (Liu et al., 2013)	$\frac{\phi(\rho-\rho_l)}{\rho+2\rho_l} + \frac{(1-\phi)(\rho-\rho_h)}{\rho+2\rho_h} = 0$	$\begin{split} F &= m_{\varphi} + \sqrt{m_{\varphi}^2 + 2\rho_h/\rho_l}, \text{ (where } m_{\varphi} = \\ & \frac{1}{2} \left[\frac{\rho_h}{\rho_l} + 3\varphi \bigg(1 - \frac{\rho_h}{\rho_l} \bigg) - 2 \right]) \end{split}$	
Maxwell–Wagner (Christensen et al., 1994)	$\rho = \rho_1 \frac{2\rho_h + \rho_l + (1 - \varphi)(\rho_h - \rho_l)}{2\rho_h + \rho_l - 2(1 - \varphi)(\rho_h - \rho_l)}$	$F = \frac{2\rho_h + \rho_1 + (1 - \phi)(\rho_h - \rho_1)}{2\rho_h + \rho_1 - 2(1 - \phi)(\rho_h - \rho_1)}$	_



of porous materials by investigating the conductivity of a porous material saturated with a single liquid, as shown in Equation 34.

$$k = c \cdot l_c^2 \frac{\sigma}{\sigma_h} \tag{34}$$

where k is permeability, c is an empirical constant (c = 1/226), and l_c is the characteristic length of pores. This model is usually applied to predict the permeability of cement-based materials. Katz and Thompson (Katz and Thompson, 1987) also established a relationship between ϕ , pore size distribution, and F to predict the permeability of cement-based materials, as shown in Equation 35, which is known as the Katz–Thompson equation (Garboczi, 1990; Bagel and Ziivica, 1997; Nokken and Hooton, 2008; Zhou et al., 2017). By combining Equation 34 and Equation 35, Equation 36 can be obtained.

$$\frac{\sigma}{\sigma_{\rm h}} = \frac{D_{\rm max}^{\rm e}}{D_{\rm c}} \cdot \phi \cdot \phi (D_{\rm max}^{\rm e}) \tag{35}$$

$$k = \frac{l_c^2}{226} \cdot \frac{D_{max}^e}{D_c} \cdot \phi \cdot \phi(D_{max}^e)$$
 (36)

where D_c is the crucial pore diameter (nm), $D_{max}^e = 0.34D_c$, and $\phi(D_{max}^e)$ is the volume fraction of pore with diameter larger than or equal to D_{max}^e . These models have been applied to investigate the pore structures of cement-based materials. According to the reported studies (Bernabé et al., 2010; Davudov et al., 2020; Xiong et al., 2020), permeability is related to the β of porous materials. Bernabé et al. (Bernabé et al., 2010) established a relationship between τ and permeability as Equation 37

$$\tau = \sqrt{\frac{4 \cdot \phi \cdot V_p^2}{k \cdot b \cdot S_p^2}}$$
 (37)

where k, b, V_p , and S_p are the permeability, geometric factor (if the pores are pipe-like, b=8 and if the pores are thin cracks, b=12), total pore volume, and total pore surface area, respectively. Then, by combining Equation 37 with Equation 30, the β of materials can be determined.

5 Numerical simulation methods for predicting the pore structure

With the rapid development of computing technology, some researchers have created several numerical simulation methods to predict the hydration, microstructure, pore structures, and mechanical properties of cement-based materials (Perko et al., 2020). Additionally, according to the shape of cement particles, these simulation methods can be divided into spherical and actual-shape numerical simulation techniques.

5.1 Spherical numerical simulation technique

Navi and Pignat (Navi and Pignat, 1996) simplified the shape of cement particles as spherical and considered the contact of particles and accessibility of water to create a simulation technique, which could be used to predict the hydration, microstructure, and pore structures of cement paste. According to transmission electron microscopy images, Bentz et al. (Bentz et al., 1995) simplified the shape of C-S-H as spherical particles and proposed a multiscale structural model to predict the microstructure and pore structures of cement paste. Subsequently, Zhang et al. (Zhang et al., 2017) used the multiscale structural model to create the microstructures of C-S-H (Figure 10), and the transport performance of the pore solution in the cement paste was calculated using electrical double layer modelling. Bishnoi and Scrivener (Bishnoi and Scrivener, 2009) considered the cement particles as spheres and proposed µic modelling platform, which uses vector and discretization approaches to simulate the microstructure and pore structures of cement-based materials.

Moreover, the hydration-morphology-structure (HYMOSTRUC) (Breugel, 1995) simulation technique simplified the shape of cement particles as spherical. This technique considers the expansion process of solid phases (see Equation 37) and penetration process of water (see Equations 38, 39) in cement paste during the hydration process.

$$\mathcal{T}_{\text{in},x,j} = \frac{x}{2} \cdot \left[1 - \sqrt[3]{1 - \alpha_{x,j}} \right] \tag{38}$$

$$\frac{\Delta \mathcal{T}_{in,x,j+1}}{\Delta t_{j+1}} = K_0(.) \cdot \Omega_1(.) \cdot \Omega_2(.) \cdot \Omega_3(.) \cdot F_1(.) \cdot \left[F_2(.) \cdot \left(\frac{\mathcal{T}_{tr}(.)}{\mathcal{T}_{x,j}} \right)^{\eta_1} \right]^{\lambda}$$
(39)

where x, $\alpha_{x,j}$, t_j , $\mathcal{T}_{in,x,j}$, $\Delta \mathcal{T}_{in,x,j+1}$, $K_0(.)$, $\mathcal{T}_{tr}(.)$, $\mathcal{T}_{x,j}$, and η_1 are the diameter of cement particles, hydration degree, hydration time, penetration depth of water, penetration depth of water during a time step of Δt_{j+1} , basic rate factor, thickness of transition layer, total thickness of total hydration product layer (when the cement

hydration is controlled by boundary, $\lambda=0$, and when the hydration is controlled by water diffusion, $\lambda=1$), and an empirical constant, respectively. In the simulation process, $K_0(.)$, $\Omega_1(.)$, $\Omega_2(.)$, $\Omega_3(.)$, and $F_1(.)$ were obtained when the hydration was controlled by boundary and water diffusion. $F_2(.)$ was calculated only for the case when the hydration was controlled by water diffusion. This simulation technique considers not only vector changing of particle volume, but also the effect of the interaction between particles on the hydration process. Moreover, the growth of the hydration products followed a dynamic process.

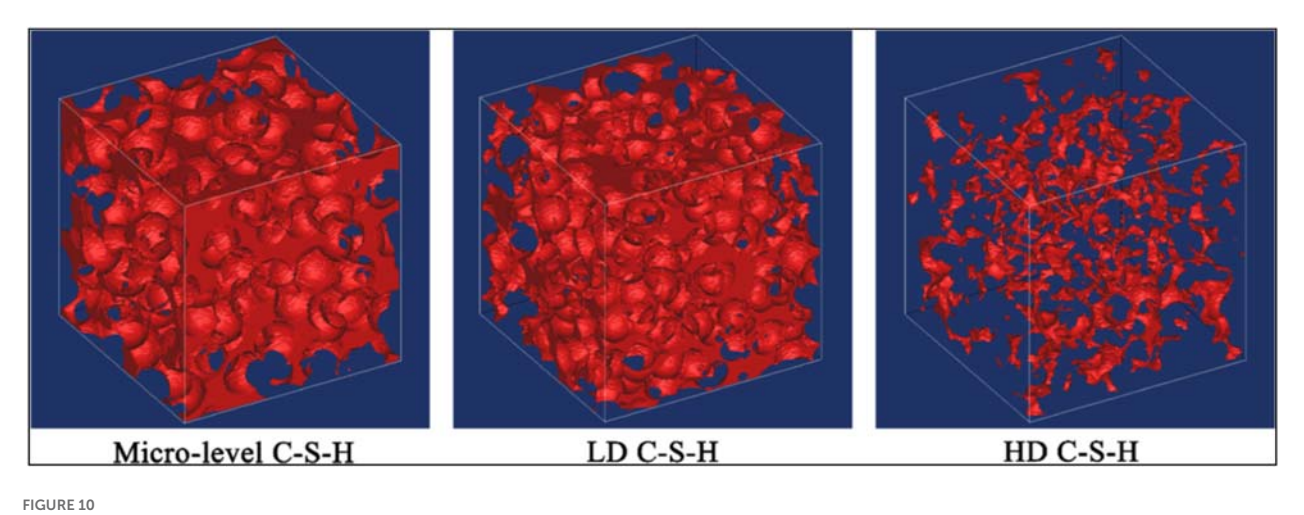
However, the actual shape of cement particles is obviously different. Liu et al. (Liu C. et al., 2018) used the improved CEMHYD3D simulation technique to study the effect of particle shape on the pore structure (ϕ , pore size distribution, and β) of cement paste and found significant effects of particle shape on the pore structures of cement paste.

5.2 Actual-shape numerical simulation technique

The CEMHYD3D simulation technique was developed by the National Institute of Standards and Technology (NIST) to describe the microstructure of cement paste during the hydration process. CEMHYD3D original code (C++) is public (Bentz, 2005). Before the modelling of CEMHYD3D, some experimental results, including the BESM image, particle size distribution, and Xray energy spectrum of cement particles, need to be obtained. Then, the principles of stereology are used to build a 3D microstructure of the cement slurry based on the experimental results. Furthermore, in CEMHYD3D, the shape of cement particles is determined by the BESM images. Therefore, in this simulation, the shape of the cement particles is closer to the actual shape of cement particles. CEMHYD3D uses the discrete cellular automata approach and biological self-replication to describe the growth of hydration products. Moreover, a voxel-based random-walk method is used to describe the diffusion process of the species in the pore solution of the cement slurry. Therefore, CEMHYD3D analyses the microstructure and pore structure of the cement slurry by controlling the growth of various hydration products. Patel et al. (Patel et al., 2018) comparatively examined and predicted the microstructure and pore structures of cement slurry using the CEMHYD3D and HYMOSTRUC techniques.

Additionally, the CEMHYD3D simulation results of cement slurry can be used as an input to finite element and finite differential models to calculate the properties such as electrical conductivity, AC impedance, permeability, and elastic modulus (Bentz et al., 1999; Bentz et al., 2000; Bentz et al., 2001; Torrents et al., 2000; Haecker et al., 2005).

To consider the dynamics of cement hydration, Bullard et al. (Bullard, 2007; Bullard et al., 2010; Bullard et al., 2015; Bullard et al., 2018; Oey et al., 2013) built the HydratiCA simulation technique to predict the microstructure of cement slurry. HydratiCA regards each solid and liquid phase in the cement slurry as an independent chemical unit (named as a cell). Therefore, this technique can directly simulate the dissolution of cement particles, the diffusion of a solute in the pore solution, the reaction of various substances in the pore solution and on the cement surface, and the nucleation-growth



Pore structures and spatial distribution of C-S-H with different densities (Zhang et al., 2017).

of hydration products. Furthermore, the principle of probability is used to simulate the chemical and structural changes in small time increments, and the increment per unit time is decomposed into transport and reaction steps. The diffusion in the cement slurry is simulated as the random motion of a cell between adjacent lattice points, and the reaction between the cells is controlled by probability (Bullard, 2007; Bullard et al., 2018) as Equation 40.

$$p_{i} = K\zeta^{\left(\sum_{q} v_{q,i}\right) - 1} \Delta t \prod_{\epsilon} \max\left(0, \prod_{m=1}^{v_{q,i}} N_{q} - m + 1\right)$$
(40)

where p_i , K, ζ , and $v_{q,i}$ are the probability of reaction, reaction rate constant, proportionality constant of the number of species q (N_q) and its molar concentration, and molar stoichiometric coefficient, respectively. Compared with other simulation techniques, HydratiCA provides more realistic simulation results of the hydration and microstructure of cement slurry; however, its unit computational cost is the largest. Once the 3D microstructure of cement-based materials is formed using numerical simulation techniques, some algorithms (such as RWA) can be employed to obtain the β of these materials (Al-Raoush and Madhoun, 2017; Liu C. et al., 2020).

6 Conclusion and research directions

Herein, we reviewed the principles, characteristics, and applications of the experimental, computational, and simulation methods used to investigate the β in cement-based materials. Through the comparative analysis of different experimental methods, some limitations of these experimental methods could be found. For example, the drying of sample in traditional methods may destroy the pore structures and solid-phase skeleton, testing the nano-scale and sub-micron pores in cement-based materials by CT is difficult due to the limitation of resolution, and the replacement of the pore solution by a pure solution (such as 3% NaCl solution (He et al., 2018)) is required for electrical methods. However, the β of cement-based materials is a key parameter to

understand the transport performance, corrosion behavior, and durability of these materials. Therefore, to accurately investigate the β in cement-based materials, some new methods need to be developed, or according to the characteristics of the existing experimental methods, an effective combination method should be established in the future.

Additionally, to date, researchers have mainly focused on the pore structures of hardened cement-based materials, and only few studies have been reported on the microstructure and pore structures of cement-based materials in the hardening stage. Nevertheless, to comprehensively understand the mechanism and prediction models of cement hydration, time-variation of the microstructure and pore structures of cement slurry in the early hydration stage should be obtained (Thomas et al., 2011). Moreover, understanding the properties of the hardening cement slurry is significant for solving the gas-migration issue of natural gas wells (Crook and Heathman, 1998; Li Z. et al., 2016; Liu et al., 2018a; Liu et al., 2019a), which threatens the safety and quality of cement engineering. Researchers (Prohaska et al., 1995; Monlouis-Bonnaire et al., 2004; Li Z. et al., 2016; Lyles, 2016) have proposed that the \beta in hardening cement slurry is crucial for studying the mechanism of gas migration and developing an anti-gas-migration technology. Compared with the hardened cement, cement slurry in the hardening stage exhibits fast hydration, low strength, and no fixed shape (Lyles, 2016), which undoubtedly increases the difficulty of investigating its pore structures. Consequently, establishing an effective method to examine the pore structures of cement slurry in the hardening stage is still a future research direction.

Nowadays, many computational models and simulation techniques are being developed to analyse the β and tortuosity of porous materials. These models and techniques have been applied to study the β in cement-based materials. However, the results obtained by these models and techniques have large errors. Therefore, through the development of experimental technologies, mathematical theories, and computing technologies, these models and techniques should be improved and some new models should be established in the future to promote the understanding of the hydration mechanism and corrosion of cement-based materials

and provide some foundation for predicting the durability of these materials and solving the engineering issues.

Author contributions

ZL: Formal Analysis, Investigation, Writing – original draft, Data curation. LJ: Formal Analysis, Investigation, Writing – original draft, Conceptualization, Funding acquisition, Resources, Supervision, Visualization, Writing – review and editing.

Funding

The author(s) declare that financial support was received for the research and/or publication of this article. PetroChina Southwest Oil & Gas Field Company Science and Technology Project (2024D102-01-16). The financial support provided by PetroChina Southwest Oil & Gas Field Company Science and Technology Project (2024D102-01-16). The funder was not involved in the study design, collection, analysis, interpretation of data, the writing of this article, or the decision to submit it for publication.

Conflict of interest

Author LJ was employed by the PetroChina Southwest Oil & Gas Field Company.

References

Abdolhosseini Qomi, M. J., Krakowiak, K. J., Bauchy, M., Stewart, K. L., Shahsavari, R., Jagannathan, D., et al. (2014). Combinatorial molecular optimization of cement hydrates. *Nat. Commun.* 5, 4960–10. doi:10.1038/ncomms5960

Al-Raoush, R. I., and Madhoun, I. T. (2017). TORT3D: a MATLAB code to compute geometric tortuosity from 3D images of unconsolidated porous media. *Powder Technol.* 320, 99–107. doi:10.1016/j.powtec.2017.06.066

Aligizaki, K. K. (2006). Pore structure of cement-based materials: testing, interpretation and requiremens. Oxfordshire, United Kingdom: Taylor and Francis.

Archie, G. E. (1941). The electrical resistivity log as an aid in determining some reservoir characteristics. *Trans. AIME* 46, 54–62. doi:10.2118/942054-g

Attari, A., McNally, C., and Richardson, M. G. (2016). A combined SEM-calorimetric approach for assessing hydration and porosity development in GGBS concrete. *Cem. Concr. Compos.* 68, 46–56. doi:10.1016/j.cemconcomp.2016. 02.001

Bagel, L., and Ziivica, V. (1997). Relationship between pore structure and permeability of hardened cement mortars: on the choice of effective pore structure parameter. Cem. Concr. Res. 27, 1225–1235. doi:10.1016/s0008-8846(97)00111-7

Barberon, F., Korb, J. P., Petit, D., Morin, V., and Bermejo, E. (2003). Probing the surface area of a cement-based material by nuclear magnetic relaxation dispersion. *Phys. Rev. Lett.* 90, 116103. doi:10.1103/PhysRevLett.90.116103

Bede, A., Scurtu, A., and Ardelean, I. (2016). NMR relaxation of molecules confined inside the cement paste pores under partially saturated conditions. *Cem. Concr. Res.* 89, 56–62. doi:10.1016/j.cemconres.2016.07.012

Bentz, D. P. (2005). CEMHYD3D: a three-dimensional cement hydration and microstructure development modeling package. doi:10.6028/NIST.IR.7232

Bentz, D. P. (2006). Influence of water-to-cement ratio on hydration kinetics: simple models based on spatial considerations. *Cem. Concr. Res.* 36, 238–244. doi:10.1016/j.cemconres.2005.04.014

Bentz, D. P., and Garboczi, E. J. (1992). Computer simulation of the diffusivity of cement-based materials. *J. Mat. Sci.* 27, 2083–2092. doi:10.1007/bf01117921

Bentz, D. P., Quenard, D. A., Baroghel-Bouny, V., Garboczi, E. J., and Jennings, H. M. (1995). Modelling drying shrinkage of cement paste and mortar part

The remaining author declares that the research was conducted in the absence of any commercial or financial relationships that could be construed as a potential conflict of interest.

Generative Al statement

The author(s) declare that no Generative AI was used in the creation of this manuscript.

Any alternative text (alt text) provided alongside figures in this article has been generated by Frontiers with the support of artificial intelligence and reasonable efforts have been made to ensure accuracy, including review by the authors wherever possible. If you identify any issues, please contact us.

Publisher's note

All claims expressed in this article are solely those of the authors and do not necessarily represent those of their affiliated organizations, or those of the publisher, the editors and the reviewers. Any product that may be evaluated in this article, or claim that may be made by its manufacturer, is not guaranteed or endorsed by the publisher.

1. Structural models from nanometres to millimetres. $Mat.\ Struct.\ 28,\ 450-458.\ doi:10.1007/BF02473164$

Bentz, D. P., Garboczi, E. J., Haecker, C. J., and Jensen, O. M. (1999). Effects of cement particle size distribution on performance properties of Portland cement-based materials. *Cem. Concr. Res.* 29, 1663–1671. doi:10.1016/S0008-8846(99)00163-5

Bentz, D. P., Jensen, O. M., Coats, A. M., and Glasser, F. P. (2000). Influence of silica fume on diffusivity in cement-based materials. *Cem. Concr. Res.* 30, 953–962. doi:10.1016/S0008-8846(00)00264-7

Bentz, D. P., Jensen, O. M., Hansen, K. K., Olesen, J. F., Stang, H., and Haecker, C. J. (2001). Influence of cement particle-size distribution on early age autogenous strains and stresses in cement-based materials. *J. Am. Ceram. Soc.* 84, 129–135. doi:10.1111/j.1151-2916.2001.tb00619.x

Bernabé, Y., Li, M., and Maineult, A. (2010). Permeability and pore connectivity: a new model based on network simulations. *J. Geophys. Res. Solid Earth* 115, 1–14. doi:10.1029/2010IB007444

Bernabé, Y., Zamora, M., Li, M., Maineult, A., and Tang, Y. B. (2011). Pore connectivity, permeability, and electrical formation factor: a new model and comparison to experimental data. *J. Geophys. Res. Solid Earth* 116, 1–15. doi:10.1029/2011JB008543

Bhattacharja, S., Moukwa, M., D'Orazio, F., Jehng, J. Y., and Halperin, W. P. (1993). Microstructure determination of cement pastes by NMR and conventional techniques. *Adv. Cem. Based Mat.* 1, 67–76. doi:10.1016/1065-7355(93)90011-C

Bishnoi, S., and Scrivener, K. L. (2009). μic: a new platform for modelling the hydration of cements. *Cem. Concr. Res.* 39, 266–274. doi:10.1016/j.cemconres.2008.12.002

Boudreau, B. P. (1996). The diffusive tortuosity of fine-grained unlithified sediments. Geochim. Cosmochim. Acta 60, 3139–3142. doi:10.1016/0016-7037(96)00158-5

Breugel, V. (1995). Numerical simulation of hydration and microstructural development in hardening cement-based materials (I) theory. *Cem. Concr. Res.* 25, 319–331. doi:10.1016/0008-8846(95)00017-8

Brunauer, S., Emmett, P. H., and Teller, E. (1938). Adsorption of gases in multimolecular layers. J. Am. Chem. Soc. 60, 309–319. doi:10.1021/ja01269a023

- Bullard, J. W. (2007). Approximate rate constants for nonideal diffusion and their application in a stochastic model. *J. Phys. Chem. A* 111, 2084–2092. doi:10.1021/jp0658391
- Bullard, J. W., Enjolras, E., George, W. L., Satterfield, S. G., and Terrill, J. E. (2010). A parallel reaction-transport model applied to cement hydration and microstructure development. *Model. Simul. Mat. Sci. Eng.* 18, 025007–025016. doi:10.1088/0965-0393/18/2/025007
- Bullard, J. W., Scherer, G. W., and Thomas, J. J. (2015). Time dependent driving forces and the kinetics of tricalcium silicate hydration. *Cem. Concr. Res.* 74, 26–34. doi:10.1016/j.cemconres.2015.03.016
- Bullard, J. W., Hagedorn, J., Ley, M. T., Hu, Q., Griffin, W., and Terrill, J. E. (2018). A critical comparison of 3D experiments and simulations of tricalcium silicate hydration. *J. Am. Ceram. Soc.* 101, 1453–1470. doi:10.1111/jace.15323
- Cao, T., Zhang, L., Sun, G., Wang, C., Zhang, Y., Yan, N., et al. (2019). Model for predicting the tortuosity of transport paths in cement-based materials. *Mater. (Basel)* 12, 3623–19. doi:10.3390/ma12213623
- Chen, S. J., Li, W. G., Ruan, C. K., Sagoe-Crentsil, K., and Duan, W. H. (2017). Pore shape analysis using centrifuge driven metal intrusion: indication on porosimetry equations, hydration and packing. *Constr. Build. Mat.* 154, 95–104. doi:10.1016/j.conbuildmat.2017.07.190
- Christensen, B. J., Coverdale, T., Olson, R. A., Ford, S. J., Garboczi, E. J., Jennings, H. M., et al. (1994). Impedance spectroscopy of hydrating cement-based materials: measurement, interpretation, and application. *J. Am. Ceram. Soc.* 77, 2789–2804. doi:10.1111/j.1151-2916.1994.tb04507.x
- Crook, B. R., and Heathman, J. (1998). Predicting potential gas-flow rates to determine best cementing practices short-term gas migration.
- Dai, T., Fang, C., Liu, T., Zheng, S., Lei, G., and Jiang, G. (2024). Waste glass powder as a high temperature stabilizer in blended oil well cement pastes: hydration, microstructure and mechanical properties. *Constr. Build. Mat.* 439, 137359. doi:10.1016/j.conbuildmat.2024.137359
- Dalas, F., Korb, J.-P., Pourchet, S., Nonat, A., Rinaldi, D., and Mosquet, M. (2014). Surface relaxivity of cement hydrates. *J. Phys. Chem. C* 118, 8387–8396. doi:10.1021/jp500055p
- Davudov, D., Moghanloo, R. G., and Zhang, Y. (2020). Interplay between pore connectivity and permeability in shale sample. *Int. J. Coal Geol.* 220, 103427. doi:10.1016/j.coal.2020.103427
- Diamond, S. (2000). Mercury porosimetry. Cem. Concr. Res. 30, 1517–1525. doi:10.1016/S0008-8846(00)00370-7
- Dong, Z., Tian, S., Xue, H., Lu, S., Liu, B., Erastova, V., et al. (2024). Analysis of pore types in Lower Cretaceous Qingshankou shale influenced by electric heating. *Energy Fuels* 38, 20577–20590. doi:10.1021/acs.energyfuels.4c03783
- Fourmentin, M., Faure, P., Rodts, S., Peter, U., Lesueur, D., Daviller, D., et al. (2017). NMR observation of water transfer between a cement paste and a porous medium. *Cem. Concr. Res.* 95, 56–64. doi:10.1016/j.cemconres.2017.02.027
- Fusseis, F., Xiao, X., Schrank, C., and De Carlo, F. (2014). A brief guide to synchrotron radiation-based microtomography in (structural) geology and rock mechanics. *J. Struct. Geol.* 65, 1–16. doi:10.1016/j.jsg.2014.02.005
- Gaitero, J. J., Campillo, I., and Guerrero, A. (2008). Reduction of the calcium leaching rate of cement paste by addition of silica nanoparticles. *Cem. Concr. Res.* 38, 1112–1118. doi:10.1016/j.cemconres.2008.03.021
- Galle, C. (2001). Effect of drying on cement-based materials pore structure as identified by mercury intrusion porosimetry: a comparative study between oven-vacuum-and freeze-drying. *Cem. Concr. Res.* 31, 1467–1477. doi:10.1016/S0008-8846(01)00594-4
- Garboczi, E. J. (1990). Permeability, diffusivity, and microstructural parameters: a critical review. Cem. Concr. Res. 20, 591–601. doi:10.1016/0008-8846(90)90101-3
- Garboczi, E. J., and Bentz, D. P. (1998). Multiscale analytical/numerical theory of the diffusivity of concrete. *Adv. Cem. based Mat.* 7, 77–88. doi:10.1016/s1065-7355(98)00010-8
- García-Macías, E., D'Alessandro, A., Castro-Triguero, R., Pérez-Mira, D., and Ubertini, F. (2017). Micromechanics modeling of the electrical conductivity of carbon nanotube cement-matrix composites. *Compos. Part B Eng.* 108, 451–469. doi:10.1016/j.compositesb.2016.10.025
- Hadley, D. W., Dolch, W. L., and Diamond, S. (2000). On the occurrence of hollow-shell hydration grains in hydrated cement paste. *Cem. Concr. Res.* 30, 1–6. doi:10.1016/S0008-8846(99)00207-0
- Haecker, C. J., Garboczi, E. J., Bullard, J. W., Bohn, R. B., Sun, Z., Shah, S. P., et al. (2005). Modeling the linear elastic properties of Portland cement paste. *Cem. Concr. Res.* 35, 1948–1960. doi:10.1016/j.cemconres.2005.05.001
- Halperin, W. P., Jehng, J.-Y., and Song, Y.-Q. (1994). Application of spin-spin relaxation to measurement of surface area and pore size distributions in a hydrating cement paste. *Magn. Reson. Imaging* 12, 169–173. doi:10.1016/0730-725X(94)91509-1
- Hansen, T. C. (1986). Physical structure of hardened cement paste. A classical approach. *Mat. Struct.* 19, 423–436. doi:10.1007/bf02472146

- Hansen, E. W., Gran, H. C., and Johannessen, E. (2005). Diffusion of water in cement paste probed by isotopic exchange experiments and PFG NMR. *Microporous Mesoporous Mater* 78, 43–52. doi:10.1016/j.micromeso.2004.09.015
- He, R., Ma, H., Hafiz, R. B., Fu, C., Jin, X., and He, J. (2018). Determining porosity and pore network connectivity of cement-based materials by a modified non-contact electrical resistivity measurement: experiment and theory. *Mat. Des.* 156, 82–92. doi:10.1016/j.matdes.2018.06.045
- Hong, S., Liu, P., Zhang, J., Xing, F., and Dong, B. (2019). Visual and quantitative identification of cracking in mortar subjected to loads using X-ray computed tomography method. *Cem. Concr. Compos.* 100, 15–24. doi:10.1016/j.cemconcomp.2019.03.010
- Hu, Q., Aboustait, M., Kim, T., Ley, M. T., Hanan, J. C., Bullard, J., et al. (2016). Direct three-dimensional observation of the microstructure and chemistry of C3S hydration. *Cem. Concr. Res.* 88, 157–169. doi:10.1016/j.cemconres.2016.07.006
- $Iversen, N., and Jørgensen, B. B. (1993). Diffusion coefficients of sulfate and methane in marine sediments: influence of porosity. {\it Geochim. Cosmochim. Acta 57, 571–578.} doi:10.1016/0016-7037(93)90368-7$
- Jiang, J., Wang, H., Lin, J., Wang, F., Liu, Z., Wang, L., et al. (2025). Nature-inspired hierarchical building materials with low CO2 emission and superior performance. *Nat. Commun.* 16, 3018–11. doi:10.1038/s41467-025-58339-8
- Karakosta, E., Lagkaditi, L., Elhardalo, S., Biotaki, A., Kelessidis, V. C., Fardis, M., et al. (2015). Pore structure evolution and strength development of G-type elastic oil well cement. A combined 1H NMR and ultrasonic study. *Cem. Concr. Res.* 72, 90–97. doi:10.1016/j.cemconres.2015.02.018
- Katz, A. J., and Thompson, A. H. (1986). Quantitative prediction of permeability in porous rock. *Phys. Rev. B* 34, 8179–8181. doi:10.1103/physrevb.34.8179
- Katz, A. J., and Thompson, A. H. (1987). Prediction of rock electrical conductivity from mercury injection measurements. *J. Geophys. Res.* 92, 599–607. doi:10.1029/JB092iB01p00599
- Keblinski, P., and Cleri, F. (2004). Contact resistance in percolating networks. *Phys. Rev. B Condens. Matter Mat. Phys.* 69, 184201–184204. doi:10.1103/PhysRevB.69.184201
- Kim, G. M., Park, S. M., Ryu, G. U., and Lee, H. K. (2017). Electrical characteristics of hierarchical conductive pathways in cementitious composites incorporating CNT and carbon fiber. *Cem. Concr. Compos.* 82, 165–175. doi:10.1016/j.cemconcomp.2017.06.004
- Koivu, V., Decain, M., Geindreau, C., Mattila, K., Bloch, J. F., and Kataja, M. (2009). Transport properties of heterogeneous materials. combining computerised X-ray micro-tomography and direct numerical simulations. *Int. J. Comut. Fluid Dyn.* 23, 713–721. doi:10.1080/10618561003727512
- Korb, J. P., Monteilhet, L., McDonald, P. J., and Mitchell, J. (2007). Microstructure and texture of hydrated cement-based materials: a proton field cycling relaxometry approach. *Cem. Concr. Res.* 37, 295–302. doi:10.1016/j.cemconres.2006.08.002
- Latour, L. L., Mitra, P. P., Kleinberg, R. L., and Sotak, C. H. (1993). Time-dependent diffusion coefficient of fluids in porous media as a probe of surface to volume ratio. *J. Magn. Reson.* A, 342–346. doi:10.1006/jmra.1993.1056
- Latour, L. L., Kleinberg, R. L., Mitra, P. P., and Sotak, C. H. (1995). Pore-size distribution and tortuosity in heterogeneous porous media. *J. Magn. Reson.* A, 83–95. doi:10.1006/jmra.1995.1012
- Li, Q., Xu, S., and Zeng, Q. (2016a). The effect of water saturation degree on the electrical properties of cement-based porous material. *Cem. Concr. Compos.* 70, 35–47. doi:10.1016/j.cemconcomp.2016.03.008
- Li, T., Shimasaki, S. I., Taniguchi, S., and Narita, S. (2016b). Reliability of inclusion statistics in steel by stereological methods. *ISIJ Int.* 56, 1625–1633. doi:10.2355/isijinternational.ISIJINT-2016-269
- Li, Z., Vandenbossche, J. M., Iannacchione, A. T., Brigham, J. C., and Kutchko, B. G. (2016c). Theory-based review of limitations with static gel strength in cement/matrix characterization. *SPE Drill. Complet.* 31, 145–158. doi:10.2118/178923-PA
- Li, N., Shi, C., Zhang, Z., Wang, H., and Liu, Y. (2019). A review on mixture design methods for geopolymer concrete. *Compos. Part B Eng.* 178, 107490. doi:10.1016/j.compositesb.2019.107490
- Li, J., Cao, S., Song, W., and Sun, L. (2025a). Visualization and quantification of pore structure in cement tailings waste rock composites using X-ray computed tomography and deep learning. *Constr. Build. Mat.* 476, 141341. doi:10.1016/j.conbuildmat.2025.141341
- Li, J., Zhang, W., Ye, J., Luo, K., Ren, X., and Lu, Z. (2025b). Mechanism of pore structure on carbonation properties of cement with high carbon fixation capacity. *Constr. Build. Mat.* 462, 139919. doi:10.1016/j.conbuildmat.2025.139919
- Liu, Z., Zhang, Y., Liu, L., and Jiang, Q. (2013). An analytical model for determining the relative electrical resistivity of cement paste and C-S-H gel. *Constr. Build. Mat.* 48, 647–655. doi:10.1016/j.conbuildmat.2013.07.020
- Liu, C., Liu, G., Liu, Z., Yang, L., Zhang, M., and Zhang, Y. (2018a). Numerical simulation of the effect of cement particle shapes on capillary pore structures in hardened cement pastes. *Constr. Build. Mat.* 173, 615–628. doi:10.1016/j.conbuildmat.2018.04.039

- Liu, K., Cheng, X., Zhang, X., Li, Z., Zhuang, J., and Guo, X. (2018b). Relationship between the microstructure/pore structure of oil-well cement and hydrostatic pressure. *Transp. Porous Media* 124, 463–478. doi:10.1007/s11242-018-1078-2
- Liu, K., Cheng, X., Gao, X., Zhang, X., Guo, X., and Zhuang, J. (2019a). Effect of the hydration rate and microstructure of Portland cement slurry on hydrostatic pressure transfer. *Powder Technol.* 352, 251–261. doi:10.1016/j.powtec.2019. 04.066
- Liu, K., Cheng, X., Li, J., Gao, X., Cao, Y., Guo, X., et al. (2019b). Effects of microstructure and pore water on electrical conductivity of cement slurry during early hydration. *Compos. Part B Eng.* 177, 107435. doi:10.1016/j.compositesb.2019.
- Liu, C., Wang, F., and Zhang, M. (2020a). Modelling of 3D microstructure and effective diffusivity of fly ash blended cement paste. *Cem. Concr. Compos.* 110, 103586. doi:10.1016/j.cemconcomp.2020.103586
- Liu, K., Cheng, X., Ma, Y., Gao, X., Yu, Y., Zhang, C., et al. (2020b). Visualization and quantification of pore structure of oil-well cement slurry in liquid-solid transition stage using high-resolution computed tomography. *Cem. Concr. Compos.* 111, 103633. doi:10.1016/j.cemconcomp.2020.103633
- Liu, K., Cheng, X., Ma, Y., Gao, X., Zhang, C., Li, Z., et al. (2020c). Analysis of interfacial nanostructure and interaction mechanisms between cellulose fibres and calcium silicate hydrates using experimental and molecular dynamics simulation data. *Appl. Sci.* 506, 144914. doi:10.1016/j.apsusc.2019.144914
- Long, W., Gu, Y., Ma, H., Li, H., and Xing, F. (2019). Mitigating the electromagnetic radiation by coupling use of waste cathode-ray tube glass and graphene oxide on cement composites. *Compos. Part B Eng.* 168, 25–33. doi:10.1016/j.compositesb.2018.12.050
- Lyles, W. A. (2016). Carbonation of cement-based materials: challenges and opportunities. Constr. Build. Mat. 120, 558–570. doi:10.1016/j.conbuildmat.2016.05.080
- MacLeod, A. J. N., Gates, W. P., and Collins, F. (2020). Durability characterisation of Portland cement-carbon nanotube nanocomposites. *Mater. (Basel)* 13, 4097. doi:10.3390/ma13184097
- McCarter, W. J., Starrs, G., Chrisp, T. M., Basheer, P. A. M., Nanukuttan, S. V., and Srinivasan, S. (2015). Conductivity/Activation energy relationships for cement-based materials undergoing cyclic thermal excursions. *J. Mat. Sci.* 50, 1129–1140. doi:10.1007/s10853-014-8669-2
- Mcdonald, P. J., Mitchell, J., and Monteilhet, L. (2005). Surface relaxation and chemical exchange in hydrating cement pastes: a two-dimensional NMR. *Phys. Rev. E* 72, 1–9. doi:10.1103/PhysRevE.72.011409
- McLachlan, D. S., Blaszkiewicz, M., and Newnham, R. E. (1990). Electrical resistivity of composites. *J. Am. Ceram. Soc.* 73, 2187–2203. doi:10.1111/j.1151-2916.1990.tb07576.x
- Mitra, P. P., Sen, P. N., Schwartz, L. M., and Le Doussal, P. (1992). Diffusion propagator as a probe of the structure of porous media. *Phys. Rev. Lett.* 68, 3555–3558. doi:10.1103/PhysRevLett.68.3555
- Monlouis-Bonnaire, J. P., Verdier, J., and Perrin, B. (2004). Prediction of the relative permeability to gas flow of cement-based materials. *Cem. Concr. Res.* 34, 737–744. doi:10.1016/S0008-8846(03)00071-1
- Moreno-Atanasio, R., Williams, R. A., and Jia, X. (2010). Combining X-ray microtomography with computer simulation for analysis of granular and porous materials. *Particuology* 8, 81–99. doi:10.1016/j.partic.2010.01.001
- Mrzygłód, B., Matusiewicz, P., Tchórz, A., and Olejarczyk-Wożeńska, I. (2013). Quantitative analysis of ductile iron microstructure a comparison of selected methods for assessment. *Arch. Foundry Eng.* 13, 59–63. doi:10.2478/afe-2013-0060
- Nakashima, Y., and Kamiya, S. (2007). Mathematica programs for the analysis of three-dimensional pore connectivity and anisotropic tortuosity of porous rocks using X-ray computed tomography image data. *J. Nucl. Sci. Technol.* 44, 1233–1247. doi:10.1080/18811248.2007.9711367
- Nakashima, Y., and Watanabe, Y. (2002). Estimate of transport properties of porous media by microfocus X-ray computed tomography and random walk simulation. *Water Resour. Res.* 38, 8-1-8–12. doi:10.1029/2001wr000937
- Navi, P., and Pignat, C. (1996). Simulation of cement hydration and the connectivity of the capillary pore space. *Adv. Cem. Based Mat.* 4, 58–67. doi:10.1016/S1065-7355(96)90052-8
- Nokken, M. R., and Hooton, R. D. (2008). Using pore parameters to estimate permeability or conductivity of concrete. *Mat. Struct. Constr.* 41, 1–16. doi:10.1617/s11527-006-9212-y
- Nybo, E., Maier, R. S., Lauchnor, E. G., Seymour, J. D., and Codd, S. L. (2019). Electrophoretic nuclear magnetic resonance measurement of electroosmotic flow and dispersion in hydrating cement paste. *Cem. Concr. Res.* 116, 11–18. doi:10.1016/j.cemconres.2018.10.028
- Oesch, T., Weise, F., Meinel, D., and Gollwitzer, C. (2018). Quantitative *in-situ* analysis of water transport in concrete completed using X-ray computed tomography. *Transp. Porous Media* 127, 371–389. doi:10.1007/s11242-018-1197-9
- Oey, T., Kumar, A., Bullard, J. W., Neithalath, N., and Sant, G. (2013). The filler effect: the influence of filler content and surface area on cementitious reaction rates. *J. Am. Ceram. Soc.* 96, 1978–1990. doi:10.1111/jace.12264

- Oh, W., and Brent Lindquist, W. (1999). Image thresholding by indicator kriging. *IEEE Trans. Pattern Anal. Mach. Intell.* 21, 590–602. doi:10.1109/34.777370
- Oh, B. H., and Jang, S. Y. (2004). Prediction of diffusivity of concrete based on simple analytic equations. *Cem. Concr. Res.* 34, 463–480. doi:10.1016/j.cemconres.2003.08.026
- Pan, X., and Gencturk, B. (2025). Gas permeability and pore structure analysis of an ultrahigh-durability oil well cement mortar plug using Micro-CT scans. *J. Mat. Civ. Eng.* 37, 04025146–18. doi:10.1061/jmcee7.mteng-19869
- Papp, V., Ardelean, I., Bulátkó, A., László, K., Csík, A., Janovics, R., et al. (2025). Effect of metakaolin and fly ash on the early hydration and pore structure of Portland cement. *Cem. Concr. Res.* 196, 107928. doi:10.1016/j.cemconres.2025.107928
- Patel, R. A., Phung, Q. T., Seetharam, S. C., Perko, J., Jacques, D., Maes, N., et al. (2016). Diffusivity of saturated ordinary Portland cement-based materials: a critical review of experimental and analytical modelling approaches. *Cem. Concr. Res.* 90, 52–72. doi:10.1016/j.cemconres.2016.09.015
- Patel, R. A., Perko, J., Jacques, D., De Schutter, G., Ye, G., and Van Breugel, K. (2018). A three-dimensional lattice boltzmann method based reactive transport model to simulate changes in cement paste microstructure due to calcium leaching. *Constr. Build. Mat.* 166, 158–170. doi:10.1016/j.conbuildmat.2018.01.114
- Patural, L., Porion, P., Van Damme, H., Govin, A., Grosseau, P., Ruot, B., et al. (2010). A pulsed field gradient and NMR imaging investigations of the water retention mechanism by cellulose ethers in mortars. *Cem. Concr. Res.* 40, 1378–1385. doi:10.1016/j.cemconres.2010.04.001
- Perko, J., Ukrainczyk, N., Šavija, B., Phung, Q. T., and Koenders, E. A. B. (2020). Influence of micro-pore connectivity and micro-fractures on calcium leaching of cement pastes-A coupled simulation approach. *Mater. (Basel)* 13, 1–23. doi:10.3390/ma13122697
- Prohaska, M., Fruhwirth, R., and Economides, M. J. (1995). Modeling early time gas migration through cement slurries. SPE Drill. Complet. 10, 178–185. doi:10.2118/27878-PA
- Provis, J. L., Myers, R. J., White, C. E., Rose, V., and Van Deventer, J. S. J. (2012). X-ray microtomography shows pore structure and tortuosity in alkali-activated binders. *Cem. Concr. Res.* 42, 855–864. doi:10.1016/j.cemconres.2012.03.004
- Pun, T. (1980). A new method for grey-level picture thresholding using the entropy of the histogram. *Signal Process.* 2, 223–237. doi:10.1016/0165-1684(80)90020-1
- Rajabipour, F., and Weiss, J. (2007). Electrical conductivity of drying cement paste. Mat. Struct. Constr. 40, 1143–1160. doi:10.1617/s11527-006-9211-z
- Ranefall, P., and Wählby, C. (2016). Global gray-level thresholding based on object size. Cytom. Part A J. Int. Soc. Anal. Cytol. 89, 385–390. doi:10.1002/cyto.a.22806
- Ridha, S., Irawan, S., and Ariwahjoedi, B. (2014). Prediction equation for permeability of class G oilwell cement under reservoir conditions. *Arab. J. Sci. Eng.* 39, 5219–5228. doi:10.1007/s13369-014-1028-4
- Ridler, T. W., and Calvard, S. (1978). Picture thresholding using an iterative selection method. *IEEE Trans. Syst. Man. Cybern.* smc-8, 630–632. doi:10.1109/TSMC.1978.4310039
- Roberts, J. N., and Schwartz, L. M. (1985). Grain consolidation and electrical conductivity in porous media. *Phys. Rev. B* 31, 5990–5997. doi:10.1103/physrevb.31.5990
- Salmas, C. E., and Androutsopoulos, G. P. (2001). A novel pore structure tortuosity concept based on nitrogen sorption hysteresis data. *Ind. Eng. Chem. Res.* 40, 721–730. doi:10.1021/ie000626y
- Sanish, K. B., Neithalath, N., and Santhanam, M. (2013). Monitoring the evolution of material structure in cement pastes and concretes using electrical property measurements. *Constr. Build. Mat.* 49, 288–297. doi:10.1016/j.conbuildmat.2013.08.038
- Sasmal, S., Ravivarman, N., Sindu, B. S., and Vignesh, K. (2017). Electrical conductivity and piezo-resistive characteristics of CNT and CNF incorporated cementitious nanocomposites under static and dynamic loading. *Compos. Part A* 100, 227–243. doi:10.1016/j.compositesa.2017.05.018
- Scrivener, K. L. (1988). The use of backscattered electron microscopy and image analysis to study the porosity of cement paste. MRS Online Proc. Libr. 137, 129–140. doi:10.1557/proc-137-129
- Shen, L., and Chen, Z. (2007). Critical review of the impact of tortuosity on diffusion. *Chem. Eng. Sci.* 62, 3748–3755. doi:10.1016/j.ces.2007.03.041
- Song, Y., Wang, J., Huang, Y., Wang, J., Weng, Y., Ma, R., et al. (2025a). Effects of varying grades/pretreatments of recycled aggregates on the development of pore structures and ITZs within reactive magnesia cement (RMC) concrete. *Cem. Concr. Res.* 190, 107782. doi:10.1016/j.cemconres.2025.107782
- Song, Y., Zhang, R., Wang, Y., Weichen, X., and Fan, L. (2025b). Permeability property study on slag-based geopolymers early-curing in corrosive environments: effects of full pore distribution, pore throat size, and connectivity. *Constr. Build. Mat.* 458, 139711. doi:10.1016/j.conbuildmat.2024.139711
- Sugiyama, T., Papel, R., Promentilla, M., Cortez, S., and Tablada, B. (2016). Evaluation of microstructure and transport properties of deteriorated cementitious materials from their X-ray Computed Tomography (CT) images. *Mater. (Basel)* 9, 388. doi:10.3390/ma9050388

- Sukop, M. C., Huang, H., Lin, C. L., Deo, M. D., Oh, K., and Miller, J. D. (2008). Distribution of multiphase fluids in porous media: Comparison between lattice Boltzmann modeling and micro-x-ray tomography. *Phys. Rev. E* 77, 026710–026717. doi:10.1103/PhvsRevE.77.026710
- Suleiman, A. R., Nelson, A. J., and Nehdi, M. L. (2019). Visualization and quantification of crack self-healing in cement-based materials incorporating different minerals. *Cem. Concr. Compos.* 103, 49–58. doi:10.1016/j.cemconcomp.2019.04.026
- Sun, H. Q., Zeng, J. J., Hong, G. Y., Zhuge, Y., Liu, Y., and Zhang, Y. (2025). 3D-printed functionally graded concrete plates: concept and bending behavior. *Eng. Struct.* 327, 119551. doi:10.1016/j.engstruct.2024.119551
- Tang, S. W., Cai, X. H., He, Z., Zhou, W., Shao, H. Y., Li, Z. J., et al. (2016). The review of pore structure evaluation in cementitious materials by electrical methods. *Constr. Build. Mat.* 117, 273–284. doi:10.1016/j.conbuildmat.2016.05.037
- Tang, S. W., Cai, X. H., He, Z., Zhou, W., Shao, H. Y., Li, Z. J., et al. (2017). The review of early hydration of cement-based materials by electrical methods. *Constr. Build. Mat.* 146, 15–29. doi:10.1016/j.conbuildmat.2017.04.073
- Thomas, J. J., Biernacki, J. J., Bullard, J. W., Bishnoi, S., Dolado, J. S., Scherer, G. W., et al. (2011). Modeling and simulation of cement hydration kinetics and microstructure development. *Cem. Concr. Res.* 41, 1257–1278. doi:10.1016/j.cemconres.2010.10.004
- Torrents, J. M., Mason, T. O., and Garboczi, E. J. (2000). Impedance spectra of fiber-reinforced cement-based composites: a modeling approach. *Cem. Concr. Res.* 30, 585–592. doi:10.1016/S0008-8846(00)00211-8
- Upshaw, M., and Cai, C. S. (2020). Critical review of recycled aggregate concrete properties, improvements, and numerical models. *J. Mat. Civ. Eng.* 32, 03120005. doi:10.1061/(asce)mt.1943-5533.0003394
- Valckenborg, R. M. E., Pel, L., Hazrati, K., Marchand, J., and Kopinga, K. (2001). Pore water distribution in mortar during drying as determined by NMR. *Mat. Struct.* 34, 599–604. doi:10.1007/bf02482126
- van Brakel, J., and Heertjes, P. M. (1974). Analysis of diffusion in macroporous media in terms of a porosity, a tortuosity and a constrictivity factor. *Int. J. Heat. Mass Transf.* 17, 1093–1103. doi:10.1016/0017-9310(74)90190-2
- Vertruyen, B., Cloots, R., Ausloos, M., Fagnard, J. F., and Vanderbemden, P. (2007). Electrical transport and percolation in magnetoresistive manganite/insulating oxide composites: case of La0.7Ca0.3MnO3/Mn3O4. *Phys. Rev. B Condens. Matter Mat. Phys.* 75, 165112–165114. doi:10.1103/PhysRevB.75.165112
- Wang, D., Wang, Q., and Huang, Z. (2019a). Investigation on the poor fluidity of electrically conductive cement-graphite paste: experiment and simulation. *Mat. Des.* 169, 107679. doi:10.1016/j.matdes.2019.107679
- Wang, W., Liu, X., Guo, L., and Duan, P. (2019b). Evaluation of properties and microstructure of cement paste blended with metakaolin subjected to high temperatures. *Mater. (Basel)* 16, 941. doi:10.3390/ma12060941
- Wang, X., Peng, Y., Wang, J., and Zeng, Q. (2019c). Pore structure damages in cement-based materials by Mercury intrusion: a non-destructive assessment by X-ray computed tomography. *Mater.* (*Basel*) 12, 2220. doi:10.3390/ma12142220
- Webber, J. B. W., Corbett, P., Semple, K. T., Ogbonnaya, U., Teel, W. S., Masiello, C. A., et al. (2013). An NMR study of porous rock and biochar containing organic material. *Microporous Mesoporous Mater* 178, 94–98. doi:10.1016/j.micromeso.2013.04.004
- Weissberg, H. (1963). Effective diffusion coefficient in porous media. $\it J. Appl. Phys.$ 34, 2636–2639. doi:10.1063/1.1729783
- Wildenschild, D., and Sheppard, A. P. (2013). X-ray imaging and analysis techniques for quantifying pore-scale structure and processes in subsurface porous medium systems. *Adv. Water Resour.* 51, 217–246. doi:10.1016/j.advwatres.2012.07.018
- Wong, H. S., Head, M. K., and Buenfeld, N. R. (2006). Pore segmentation of cement-based materials from backscattered electron images. *Cem. Concr. Res.* 36, 1083–1090. doi:10.1016/j.cemconres.2005.10.006
- Woo, L. Y., Wansom, S., Ozyurt, N., Mu, B., Shah, S. P., and Mason, T. O. (2005). Characterizing fiber dispersion in cement composites using AC-Impedance Spectroscopy. *Cem. Concr. Compos.* 27, 627–636. doi:10.1016/j.cemconcomp.2004.06.003
- Xiao, L., and Li, Z. (2008). Early-age hydration of fresh concrete monitored by non-contact electrical resistivity measurement. *Cem. Concr. Res.* 38, 312–319. doi:10.1016/j.cemconres.2007.09.027
- Xiong, F., Sun, W., Ba, J., and Carcione, J. M. (2020). Effects of fluid rheology and pore connectivity on rock permeability based on a network model. *J. Geophys. Res. Solid Earth* 125. doi:10.1029/2019JB018857
- Xu, J., Wu, S., Liu, J., Yuan, Y., Cui, J., Su, L., et al. (2021). New insights into controlling factors of pore evolution in organic-rich shale. *Energy Fuels* 35, 4858–4873. doi:10.1021/acs.energyfuels.0c04189
- Yang, K., Li, M., Ling, N. N. A., May, E. F., Connolly, P. R. J., Esteban, L., et al. (2019a). Quantitative tortuosity measurements of Carbonate rocks using pulsed field gradient NMR. *Transp. Porous Media* 130, 847–865. doi:10.1007/s11242-019-01341-8
- Yang, X., Kuru, E., Gingras, M., and Iremonger, S. (2019b). CT-CFD integrated investigation into porosity and permeability of neat early-age well cement at downhole condition. *Constr. Build. Mat.* 205, 73–86. doi:10.1016/j.conbuildmat.2019.02.004

- Ye, G., Hu, J., Van Breugel, K., and Stroeven, P. (2002). Characterization of the development of microstructure and porosity of cement-based materials by numerical simulation and ESEM image analysis. *Mat. Struct. Constr.* 35, 603–613. doi:10.1007/bf02480353
- Yu, J., Wang, H., Sun, X., Chen, Z., and Dong, W. (2024). Characterizing connectivity and tortuosity of pore network based on LF-NMR method to assess the water permeability of white cement mortar. *J. Build. Eng.* 93, 109862. doi:10.1016/j.jobe.2024.109862
- Yue, Z., Su, Z., Paul, P. P., Marsh, A. T. M., Macente, A., Di Michiel, M., et al. (2025). 3D crystalline phase and pore structure evolution upon CO2 exposure in sodium sulfate-activated cement pastes. *Cem. Concr. Res.* 187, 107716. doi:10.1016/j.cemconres.2024.107716
- Zecca, M., Vogt, S. J., Connolly, P. R. J., May, E. F., and Johns, M. L. (2018). NMR measurements of tortuosity in partially saturated porous media. *Transp. Porous Media* 125, 271–288. doi:10.1007/s11242-018-1118-y
- Zeng, Q., Li, K., Fen-Chong, T., and Dangla, P. (2012). Analysis of pore structure, contact angle and pore entrapment of blended cement pastes from mercury porosimetry data. *Cem. Concr. Compos.* 34, 1053–1060. doi:10.1016/j.cemconcomp.2012.06.005
- Zhang, J. (2008). Microstructure study of cementitious materials using resistivity measurement.
- Zhang, M. (2017). Pore-scale modelling of relative permeability of cementitious materials using X-ray computed microtomography images. *Cem. Concr. Res.* 95, 18–29. doi:10.1016/j.cemconres.2017.02.005
- Zhang, M., and Jivkov, A. P. (2016). Micromechanical modelling of deformation and fracture of hydrating cement paste using X-ray computed tomography characterisation. *Compos. Part B Eng.* 88, 64–72. doi:10.1016/j.compositesb.2015.11.007
- Zhang, J., and Li, Z. (2009). Application of GEM equation in microstructure characterization of cement-based materials. *J. Mat. Civ. Eng.* 21, 648–656. doi:10.1061/(ASCE)0899-1561(2009)21:11(648)
- Zhang, J., and Scherer, G. W. (2011). Comparison of methods for arresting hydration of cement. Cem. Concr. Res. 41, 1024–1036. doi:10.1016/j.cemconres.2011.06.003
- Zhang, Y., and Zhang, M. (2014). Transport properties in unsaturated cement-based materials a review. *Constr. Build. Mat.* 72, 367–379. doi:10.1016/j.conbuildmat.2014.09.037
- Zhang, M., He, Y., Ye, G., Lange, D. A., and Breugel, K. V. (2012). Computational investigation on mass diffusivity in Portland cement paste based on X-ray computed microtomography (µCT) image. Constr. Build. Mat. 27, 472–481. doi:10.1016/j.conbuildmat.2011.07.017
- Zhang, Y., Liu, C., Liu, Z., Liu, G., and Yang, L. (2017). Modelling of diffusion behavior of ions in low-density and high-density calcium silicate hydrate. *Constr. Build. Mat.* 155, 965–980. doi:10.1016/j.conbuildmat.2017.08.128
- Zhang, P., Lu, S., Li, J., Chen, C., Xue, H., and Zhang, J. (2018a). Petrophysical characterization of oil-bearing shales by low-field nuclear magnetic resonance (NMR). *Mar. Pet. Geol.* 89, 775–785. doi:10.1016/j.marpetgeo.2017.11.015
- Zhang, P., Wittmann, F. H., Lura, P., Müller, H. S., Han, S., and Zhao, T. (2018b). Application of neutron imaging to investigate fundamental aspects of durability of cement-based materials: a review. *Cem. Concr. Res.* 108, 152–166. doi:10.1016/j.cemconres.2018.03.003
- Zhang, P., Zheng, Y., Wang, K., and Zhang, J. (2018c). A review on properties of fresh and hardened geopolymer mortar. *Compos. Part B Eng.* 152, 79–95. doi:10.1016/j.compositesb.2018.06.031
- Zhang, Z., Zhu, Y., Zhu, H., Zhang, Y., Provis, J. L., and Wang, H. (2019). Effect of drying procedures on pore structure and phase evolution of alkali-activated cements. *Cem. Concr. Compos.* 96, 194–203. doi:10.1016/j.cemconcomp.2018.12.003
- Zhang, W., Zheng, Q., Ashour, A., and Han, B. (2020a). Self-healing cement concrete composites for resilient infrastructures: a review. *Compos. Part B Eng.* 189, 107892. doi:10.1016/j.compositesb.2020.107892
- Zhang, X., Yang, J., Li, K., Pu, H., Meng, X., Zhang, H., et al. (2020b). Effects of steam on the compressive strength and microstructure of cement paste cured under alternating ultrahigh temperature. *Cem. Concr. Compos.* 112, 103681. doi:10.1016/j.cemconcomp.2020.103681
- Zhou, B., Han, Q., and Yang, P. (2016). Characterization of nanoporous systems in gas shales by low field NMR cryoporometry. *Energy and Fuels* 30, 9122–9131. doi:10.1021/acs.energyfuels.6b01780
- Zhou, C., Ren, F., Wang, Z., Chen, W., and Wang, W. (2017). Why permeability to water is anomalously lower than that to many other fluids for cement-based material? *Cem. Concr. Res.* 100, 373–384. doi:10.1016/j.cemconres.2017.08.002
- Zhou, C., Ren, F., Zeng, Q., Xiao, L., and Wang, W. (2018). Pore-size resolved water vapor adsorption kinetics of white cement mortars as viewed from proton NMR relaxation. *Cem. Concr. Res.* 105, 31–43. doi:10.1016/j.cemconres.2017.12.002
- Zhu, X., Zhang, Z., Yang, K., Magee, B., Wang, Y., Yu, L., et al. (2018). Characterisation of pore structure development of alkali-activated slag cement during early hydration using electrical responses. *Cem. Concr. Compos.* 89, 139–149. doi:10.1016/j.cemconcomp.2018.02.016